Functional and pathophysiological study of disease processes in humans and animal systems: Role of magnetic resonance imaging and *in vivo* MR spectroscopy*

N. R. Jagannathan
Department of NMR, All India Institute of Medical Sciences, New Delhi 110 029, India

Magnetic resonance imaging (MRI), a non-invasive imaging modality, has revolutionized the field of clinical medicine with its multiplanar imaging capability, high spatial resolution, excellent soft tissue contrast and absence of ionizing radiation. It covers a broad range of applications from fast noninvasive anatomical measurements to the study of tissue physiology and metabolism.

MR images arise primarily from the protons of water and fat present in human and/or animal tissues. Several variants of MR methods have been developed for studying specific disease processes. Recently, diffusion and perfusion MRI have found widespread application in the evaluation of epilepsy, stroke and other brain disorders. Functional MRI, yet another advance, is useful for studying several brain functions and has immense potential in unravelling the mystery of the human brain. It has the capability of identifying specific anatomical sites involved in many cognitive processes. Another aspect of MR is the so-called *in vivo* MR spectroscopy of living systems. *In vivo* MRS of living systems are an extension of the traditional high-resolution NMR method used for studying structure of molecules but applied to more complex systems. Among the various nuclei that generate MR signal, proton (^{1}H) and phosphorous (^{31}P) are important in the study of the biochemistry of living systems. *In vivo* MRS can be used to observe different biochemicals (metabolites) from a particular specified region of a living system. Determination of the concentration and relative levels of these metabolites provides information on the normal and abnormal states of tissues and their response to various therapeutic modalities. In short, *in vivo* MRS can be used as a unique means for probing the biochemistry and physiology of living systems.

In this article, a general overview of the basics, development and the applications of various MRI and MRS methodologies used in clinical and experimental research are presented to understand the pathophysiology of various disease processes.

ADVANCES in medical imaging techniques have revolutionized the area of clinical medicine with the use of X-rays, CT, MRI, SPECT and PET scans which allow us to probe the human body to diagnose, monitor or guide treatment of a variety of diseases and injuries. The field of medical imaging began with Wilhelm Roentgen's discovery of X-rays in 1895 and in fact, until the early 1970s, it was the only technique available for imaging. Although X-rays are useful for delineating the bones, they do not provide detailed information about the soft tissues of the human body. A major advance was made in mid-1970s with the development of computerized tomography (CT) using X-rays, which can image head as well as other parts of the body, relatively quickly.

Although CT opened a new era in imaging, almost at the same time MRI revolutionized the field of diagnostic radiology by providing detailed high-resolution images of different structures of internal organs of the human body. MRI produces a series of cross-sectional images in any desired plane of any region of the body. Unlike CT, MRI uses a strong magnet and radio waves rather than X-rays to produce its images. Though more time consuming than the CT scan, it has the best soft tissue characterization among all the existing imaging techniques. MRI is superior to CT in that patients are not exposed to X-rays and images can be taken along any angle through the body.

MRI is an extension of the more generalized phenomenon called nuclear magnetic resonance (NMR). Magnetic resonance (MR) is the study of the interaction of a molecule (to be precise atomic nuclei such as hydrogen) with radiofrequency (RF) field in the presence of an external magnetic field, $\mathbf{B_0}$. Hydrogen is the most commonly used nuclei for medical imaging because of its wide distribution in biological tissues. The development of MRI started with the work of Damadian who demonstrated that the NMR relaxation time constants (T1 and T2) are different for normal and malignant tissues and could have diagnostic

*Presented at the 14th mid-year meeting of the Indian Academy of Sciences, July 2003, Bangalore.
e-mail: jagan1954@hotmail.com

value[1]. In 1973, Lauterbur produced the first NMR image of an object and called it 'zeugmatography', using magnetic field gradients[2]. Later, MR images of human organs like finger[3], hand[4] and wrist[5] were reported. With the developments in magnet technology, RF electronics and powerful computers in mid-1980s, the full potential of magnetic resonance imaging (MRI) as a clinical tool was realized. In the last two decades MRI has experienced rapid expansion and has achieved on amazing level of success as an important tool to study several disease processes in clinical and experimental research. Recent advances in MRI methodology offer high spatial resolution (100 μm or less), enabling detailed morphological/anatomical information to be obtained from small animals. This rapid growth is due to its noninvasive nature, avoidance of ionizing radiation and its ability to generate high-resolution images. Recently, Lauterbur and Mansfield were awarded the Nobel Prize for their seminal contribution 'concerning the use of MR to visualize different structures' (Box 1).

In vivo MR spectroscopy (MRS) of cells and of organs of living systems are an extension of high-resolution NMR used for studying structure of molecules, but applied to more complex systems. It can be used to observe different metabolites present in a particular region of tissues and organs. The determination of the concentration and relative levels of these metabolites provide information on the normal and abnormal tissues. The method is useful to monitor the response of tumours to various therapeutic modalities and to understand the different metabolic processes[6,7]. Thus, *in vivo* MRS can be used as a unique means for probing the biochemistry of living systems and is increasingly being used in clinical, experimental, pharmaceutical and biological research. It serves as a link between clinical and pre-clinical applications that renders it as an attractive tool[7]. Even though for a number of reasons MRI and MRS have evolved more or less independently, *in vivo* localized MRS in human and other living systems, are mainly guided through MR images. Thus, the success of MRI has led to considerable interest in MRS as a noninvasive probe for monitoring the metabolism of living systems. In this article, an overview of the potential of MRI and *in vivo* MRS in understanding the pathophysiology of several disease processes is presented.

Image formation

Water constitutes 70% of the human body weight and most MR images are acquired using the hydrogen (proton) nuclei present in the water molecule. There are differences in water content among tissues and organs and in many diseases the pathological processes alter the characteristics of water, which is reflected in the MR image. Each water molecule has two hydrogen atoms covalently bound to an oxygen atom and there are approximately 5×10^{27} hydrogen nuclei in an adult human body that are randomly oriented. These nuclei behave as tiny magnets (magnetic dipoles) and when a human body is exposed to a strong magnetic field, these line-up either parallel or anti-parallel to $\mathbf{B_0}$. More spins will be in the parallel orientation since this is the lower energy state. With the application of an appropriate RF field, these nuclei return to parallel state emitting RF energy (NMR signal), which depends on the strength of the applied external magnetic field. This relationship is expressed by Larmor equation:

$$\nu_0 = (\gamma/2\pi)\mathbf{B_0},$$

where ν_0 is the resonance frequency expressed in MHz and γ the gyromagnetic ratio in units of frequency/field strength, is a nuclear property. Thus the resonance phenomenon is governed by a simple relation between strength of the magnetic field and frequency of radio waves.

In MRI, the magnetic field strength across the body is manipulated, such that different tissues of the body can be labelled with different frequencies. Thus, if a linear gradient G is applied in the direction x along with the large static field $\mathbf{B_0}$, then

$$\nu = (\gamma/2\pi)\ \mathbf{B_0}\ (1 + G_x)$$

and the observed frequency can measure the value of x. A linear gradient in any one of the three orthogonal directions, x, y, or z or by using combinations of these gradients, the overall gradient could be set in any chosen direction[2]. The images are pictorial representation of the spatial distribution of mobile protons in the body that arise primarily from water and fat. The density of mobile protons in tissues affects the image contrast in addition to other factors to be discussed later in this article. The principles of MRI and *in vivo* MRS are described in many textbooks[6–12].

MRI systems are generally characterized by strength of the magnetic field and imaging is generally performed with field strengths in the range of 0.2 to 2 Tesla, although imaging outside this range is possible. The strength of the magnetic field determines the tissue (proton) resonant frequency. Prior to the actual image acquisition, the magnetic field is the same at all points throughout the region, say, a patient's body. However during the acquisition, the gradient magnetic fields (discussed above) are switched on in a pulsed fashion. The gradient coils are situated within the bore of the magnet. The gradient coils consist of three pairs: x-, y-, and z-gradients. z-gradient changes the magnetic field along the z-axis, thereby allowing a slice of the patient to be selected for imaging. x-gradient coils produce a magnetic field gradient across the patient, thus providing spatial localization along the x-axis of the patient called as 'frequency encoding'. The y-gradient coils produce magnetic field gradient through the patient from front to back, and by convention, the y-axis is the vertical axis through the patient used for 'phase encoding' the MR signal. Together, the y- and x-gradients allow precise determination of where within the imaging plane the contribution to the NMR signal from each voxel or pixel

Box 1. Nobel Prize for Physiology or Medicine, 2003

Nuclear magnetic resonance (NMR) discovered as a technique for various applications of physics initially, soon found widespread application as a method of structure elucidation of organic and biological molecules in 1970s. During the same time NMR moved into a totally new area for obtaining 'spatial' information of objects that had great potential in the fields of medicine and biology. The 2003 Nobel Prize for Physiology or Medicine was awarded jointly to Paul C. Lauterbur and Peter Mansfield for their discoveries concerning 'magnetic resonance imaging'. Lauterbur discovered the possibility to create a two-dimensional picture by introducing gradients in the main static magnetic field. In 1973, he described how addition of gradient magnetic field to the main magnet made it possible to visualize the cross-section of tubes (or other origin) with water. This made it possible to create two-dimensional pictures of structures that could not be visualized with other methods. Mansfield utilized gradients in the magnetic field in order to more precisely show differences in the resonance. He mathematically analysed the NMR signal and showed how the detected signals could rapidly and effectively be transformed to an image. Mansfield also proposed a fast imaging method that could be achieved by single excitation pulse followed by rapid switching of a strong gradient.

Paul C. Lauterbur was born on 6 May 1929 in Sidney, Ohio, USA. He obtained his B Sc in Chemistry in 1951 and his Ph D in Chemistry in 1962 from the University of Pittsburg, Pennsylvania, USA. He was Research Associate at the Mellon Institute from 1951 to 1963 and later a Faculty at the State University of New York, Stony Brook from 1969 to 1985. Presently he is the Professor and Director, Biomedical MR Laboratory, University of Illinois, College of Medicine at Urbana-Champaign, IL, USA. He won numerous awards in Chemistry, Physics and Biomedical Sciences. His initial research interest includes work on carbon-13, silicon-29 and other nuclei. In 1971, he conceived the idea of using magnetic field gradients to obtain two- or three-dimensional spatial information about the distribution of magnetic nuclei in a sample placed inside a NMR coil and thus to create a 'picture' of the object by NMR. The Larmor relation $\nu_0 = (\gamma/2\pi)\mathbf{B_n}$ ensured that the NMR frequency would precisely monitor the magnetic field $\mathbf{B_n}$ at the nucleus, so that if a linear gradient G is applied in the direction x, along with the large static field $\mathbf{B_0}$, then $\nu = (\gamma/2\pi)\mathbf{B_0}(1 \pm G_x)$, and the observed frequency can measure the value of x. Lauterbur realized that a linear gradient in any one of the three orthogonal directions, x, y, or z or by using combinations of these Cartesians gradients, the overall gradient could be set in any chosen direction. This seminal contribution appeared in *Nature* in March 1973. This paper illustrates the use of gradients in several directions and by back-projecting the one-dimensional spectrum, a two-dimensional image of two capillaries of water, which would fit within a standard 5-mm diameter, was generated. The image formation from NMR is different from that of classical laws of diffraction in that it is the combined effect of the static magnetic field and the RF that leads to localization. He coined the term 'zeugmatography', which in Greek means 'that which is used for joining'. Lauterbur tested a number of other small objects and the first living animal to be imaged was a clam, 4-mm in diameter, which fitted into a standard 5-mm sample NMR tube. The NMR image showed the soft structure within the closed shell, the latter not contributing to the proton signal[b]. Later in 1974 an image of the thoracic cavity of a living mouse was demonstrated[c].

Peter Mansfield born on 9 October 1933 in England, obtained his B Sc in 1959 and Ph.D. in Physics from the University of London in 1962. He worked as a Research Associate at the University of Illinois, USA from 1960 to 1964. Later, he moved as a Faculty to the Department of Physics, University of Nottingham, England where he rose to become a Professor in 1979. He won numerous awards including Fellow of the Royal Society (FRS) and was Knighted in 1993. His early research interests were in multiple pulse techniques for line narrowing in solids. In 1970s Mansfield and Grannell reported a one-dimensional interferogram to a resolution of better than 1 mm from layers of camphor using magnetic fields gradients[d,e]. The pulsed approach proposed by them had an optical analogy of plane-wave scattering through mathematical framework where reciprocal lattice space or k-space was introduced and in which the **k** vector was proportional to the product of time and gradient vector. The concept of k-space in MRI, of course, now plays an important role in categorizing different imaging sequences in terms of the k-space trajectory. They pointed out that NMR diffraction could be useful at the macroscopic level for microscopy in biophysical systems with regular, or approximately regular macroscopic structures, e.g. cell membranes and filamentary or fibre structures[d]. Mansfield and his workers examined the theory and reported one-dimensional responses and 2D images obtained by projection–reconstruction techniques. Later they worked on switched gradient methods with selective-pulse excitation[f] to define a strip within the slice and obtain an image a 'line' at a time[g,h]. Using this method they produced a cross-sectional image of human finger—the first image to reveal anatomical detail in a live human object[e].

In 1977 Mansfield reported ultra-high-speed imaging method which was eventually named as 'echo-planar imaging' or EPI[i]. In this method, the entire slice selection was obtained with one excitation RF pulse followed by a string of echoes that resulted from a rapid and repeated switching of field gradients. This gives series of gradient echoes, each of which is given a different degree of phase encoding and thus can be reconstructed to form an image. Using this methodology, Mansfield and Pykett obtained crude images of a phantom[k] and of anatomical features[l,m]. In 1981, the first real-time moving images were obtained, which demonstrated the potential for 'freezing' cardiac motion[n].

By mid-1980s, added by developments in magnet technology, RF electronics, powerful computers, and image processing algorithms the full potential application of MRI in the diagnosis of various diseases like tumours and cancers was realized and has now become an indispensable tool in clinical medicine. A great advantage with MRI is that it is harmless and does not use ionizing radiation, in contrast to X-ray or CT scan. In addition to its use as a diagnostic tool, MRI examinations have also become important in treatment and follow-up of various disease processes. It can also be used to ascertain the stage of a tumour, which is important for the choice of treatment. In fact, MRI replaced several invasive examinations, thereby reducing the suffering of many patients. An estimated 22,000 MRI scanners are in use worldwide and more than 60 million MRI examinations have been performed.

a. Lauterbur, P. C., *Nature*, 1973, **242**, 190.
b. Lauterbur, P. C., In *Proceedings of the first International Conference on Stable Isotopes in Chemistry, Biology and Medicine* (eds Klein, P. D. and Peterson, S. V.), Argonne National Laboratory, Argonne, IL, 1973, pp. 255–260.
c. Lauterbur, P. C., *Pure Appl. Chem.*, 1974, **40**, 149.
d. Mansfield, P. and Grannell, P. K., *J. Phys. C*, 1973, **6**, L442.
e. Mansfield, P., Grannell, P. K., Garroway, A. N. and Stalker, D. C., 1st Specialized Colleague AMPERE, Karakow, 1973, p. 16.
f. Garroway, A. N., Grannell, P. K. and Mansfield, P., *J. Phys. C*, 1974, **7**, L457.
g. Mansfield, P. Maudsley, A. A. and Baines, T., *J. Phys. E*, 1976, **9**, 271.
h. Mansfield, P. and Maudsley, A. A., *Phys. Med. Biol.*, 1976, **21**, 847.
i. Mansfield, P. and Maudsley, A. A., *Br. J. Radiol.*, 1977, **50**, 847.
j. Mansfield, P., *J. Phys. C*, 1977, **10**, L55.
k. Mansfield, P. and Pykett, I. L., *J. Magn. Reson.*, 1978, **29**, 355.
l. Mansfield, P. and Pykett, I. L., *Abstr. 19th Exp. NMR Conf. Blacksburg*, VA, 1978.
m. Mansfield, P. and Morris, P. G., Ordidge, R. J., Pykett, I. L., Bangut, V. and Coupland, R. F., *Philos. Trans. R. Soc. London*, 1980, **B289**, 503.
n. Ordidge, R. J., Mansfield, P., Doyle, M. and Coupland, R. F., *Radiology*, 1982, **142**, 244.

originates. The z-gradient is always used for selection of a transaxial plane to be imaged and is called 'slice selection'. To select either the axial, sagittal or coronal plane for imaging, the z-, x- or y-gradients respectively, will be energized as magnetic fields add vectorially. When all the three gradients are energized at the same time, an oblique plane is defined. Thus, the purpose of these gradient magnetic fields is two-fold: slice selection and pixel localization within the slice. The combination of a field gradient inhomogeneity and excitation by a specific frequency permits slice selection. The presence of a gradient field during relaxation helps to localize the protons within the slice that was selected during excitation. The steeper the gradient field, the thinner will be the slice. Similarly, narrow bandwidth RF pulses, produces thinner slices.

Normally, MR images are either T1- or T2-weighted. T1 and T2 refer to magnetic resonance time constants that are intrinsic to a given tissue. T1 is the spin-lattice (longitudinal) relaxation time. As the nuclei return to the lower energy state, that is, relax; energy is lost by interaction with the surrounding lattice or environment. T2 denotes the spin–spin (transverse) relaxation time. This refers to the loss of energy due to interaction with other nuclei aligned with the magnetic field. T2 relaxation is actually confounded by T2* relaxation, which is much shorter and results from inhomogeneity in the magnetic field. While T1 and T2 relaxation times have been separated for purposes of discussion, it is important to realize that they are occurring simultaneously during any given imaging procedure, and both are contributing some relative amount to the imaging process. T1 and T2 are specific tissue characteristics. Their value will vary depending on other factors such as magnetic field strength. Nevertheless, at a given field strength, different tissues have different characteristic T1s and T2s (see Table 1).

The primary sources of inherent tissue contrast in MRI are three-fold: proton (spin) density (PD), T1 and T2. While PD within soft tissue varies by only a few per cent, the proton contribution to the measured MR signal tends to vary by a greater amount, from a few per cent up to 30% among soft tissues. Further, T1 and T2 relaxation times often vary even more widely, sometimes by more than 100% among soft tissues (Table 1), and can have important effect on image contrast. For example, the T1 of CSF is several times greater than white matter. Similarly, oedema has higher T1 and T2 than normal white matter. A few types of lesions, such as lipomas, melanomas and fibrous lesions deviate from this general rule of having higher T1 and T2 values than the surrounding normal tissues.

Table 1. Relaxation times T1 and T2 at field strength of 1.0 Tesla for various tissues together with proton density (PD)

Tissue	PD (%)	T1(ms)	T2(ms)
Brain grey matter	69	520	90
Brain white matter	61	390	90
Fat	90	180	90
Skeletal muscle	100	600	40
CSF	100	2000	300
Oedema	86	900	77
Blood	90	800	180
Spleen	92	480	80
Liver	91	270	50
Water	100	2500	2500

Applications of MRI

The techniques of MR imaging have advanced considerably in the last two decades and the pace of innovation has been rapid. Developments like high power gradient systems and optimized coil technology have allowed improvements in spatial resolution and signal-to-noise and better cost effectiveness of MR studies. This has led to improved diagnosis in shorter period of time and better understanding of complex disease processes.

MR has become a versatile and virtually indispensable imaging modality for CNS, cardiac, and other musculoskeletal applications[6,13]. Owing to excellent soft tissue contrast, even small structures are clearly seen, for example, the cranial nerves. Tumours, demyelinating disease and other pathologies show good contrast on T2-weighted images (Figure 1). Because of the absence of artifacts due to bones, MRI is the method of choice of imaging of the vertex, posterior fossa, walls of the middle fossa at

Figure 1. T2-weighted transverse (axial) spin-echo MR image of a patient suffering from anaplastic astrocytoma (slice thickness = 5 mm; TR = 2600 ms; TE = 90 ms; FOV = 250 mm).

the base of the skull, and for orbits. MRI demonstrates smaller tumours better than CT and in a majority of cases without the use of contrast material. The method is useful for evaluating acoustic neuromas, pituitary tumours, non-neoplastic disease, ischaemia, haemorrhage, arteriovenous malformations, trauma, disorders of myelination, dementia, infection, etc. The applications of MRI for the study of spine are numerous and the normal anatomy of the spine is best defined in sagittal plane (Figure 2). The application of MRI in the musculoskeletal systems includes imaging of articular cartilage, abdomen, pelvis, shoulder, wrist, knee, and musculoskeletal tumours and infections.

Cardiac MRI

With the development of ultra-fast imaging techniques and high magnetic field gradients, cardiac MRI has emerged as a powerful tool in diagnostic radiology. Most cardiac images are obtained using ECG triggering or pulse triggering to avoid image artifacts due to heart motion. ECG triggering uses the electrical signal of the heart to monitor the progression of the heart cycle. The R-wave is used as a reference for starting MRI measurements and a freely selectable delay time can be chosen to measure various stages of the cardiac cycle. This method of motion artifact suppression is useful to eliminate any image blurring due to heart contractions. Pulse triggering works in a similar way. The pulse pressure at the fingertip serves as synchronization signal. Motion and flow artifacts are suppressed with pulse triggering. This method is less complex than ECG triggering and facilitates routine examinations of the heart.

The clinical uses include imaging of cardiac morphology (Figure 3 – showing the four chambers of the heart); myocardial ischaemia, infarct and imaging of wall motion deficits. It is well suited as a first line imaging modality for evaluation of the diseases of the great vessels (e.g. aortic dissection, aneurysm, coarctation, etc.). Multi-planar reconstruction can be used to clarify the spatial course of the vascular structures. MR is also good for evaluating effusions, haematomas and intramural processes. Further, information about morphology and function can be obtained by using a CINE sequence, which acquires dynamic images of the heart over the cardiac cycle. This technique can also be used for evaluating valve function, i.e. a stenosis or insufficiency, and to visualize complicated morphological and blood flow-dependent effects.

MRI can be used for accurate assessment of ventricular function and all parts of the myocardial wall can be imaged with high temporal and high spatial resolution. Further, the quantification of ejection fraction, stroke volume, and cardiac output are less operator-dependent than with echocardiography. Multi-slice short axis coverage of the whole heart eliminates the geometric assumptions involved in ultrasound measurements. With fast real-time imaging, it is possible to scan the whole heart in one single breath-hold and with free breathing.

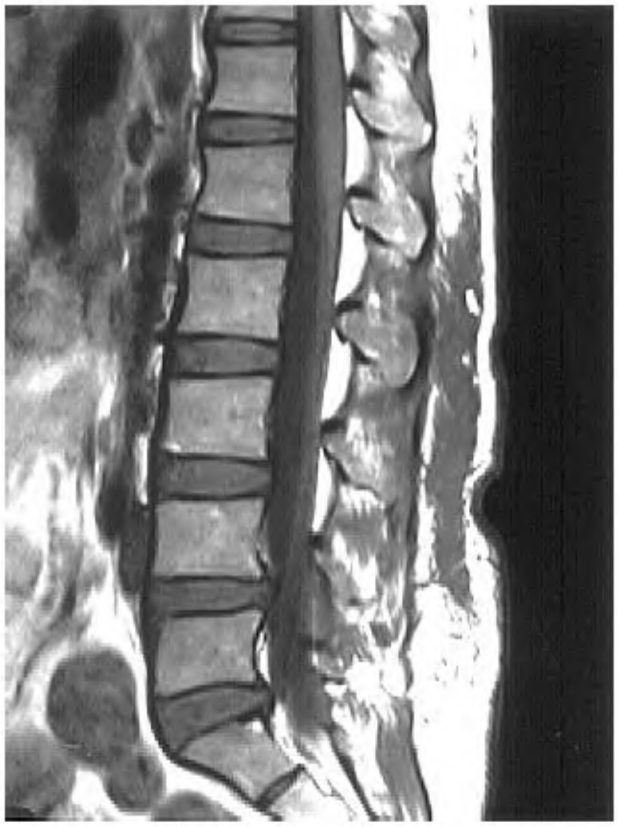

Figure 2. T2-weighted sagittal image (TR = 2800 ms; TE = 90 ms, FOV = 400 mm) of whole spine.

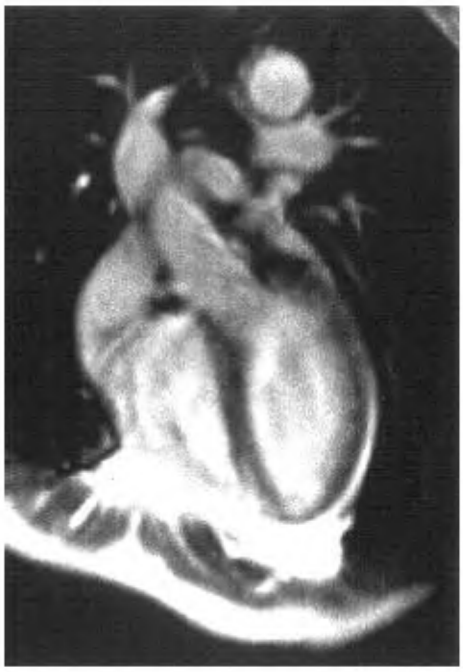

Figure 3. T2-weighted MR image of the myocardium showing the four chambers of the heart obtained using TRUE-FISP sequence.

3D coronary MRA and respiratory motion corrected techniques with the use of navigator echoes have been developed. The MR viability technique is a fast and robust method to identify the location and the extent of an infarct. The technique provides good spatial resolution and is sensitive in detecting even small infarcts. With the use of ultra-short repetition time, it is possible to perform 3D volumetric acquisitions with 1 s temporal resolution which are useful in high temporal resolution pulmonary and carotid MRA.

Magnetic resonance angiography

It is known that MRI is sensitive to motion resulting in a variety of flow effects. On one hand, flow effects are responsible for a number of artifacts, which can drastically impair the diagnostic value of the images; on the other hand, flow effects can be used advantageously to develop noninvasive techniques for imaging of the vascular anatomy. These techniques are referred to as *magnetic resonance angiography* (MRA) and are a physiologic record of blood flow[14]. MRA techniques are classified into two major categories: time-of-flight (TOF) and phase-contrast (PC) MR angiography. Both rely on separate physical effects, and will result in different images with different information about the vasculature. TOF is dependent on T1 contrast mechanisms while PC emphasizes T2 tissue differences. Using dark blood MRA method it is possible to visualize both the vessels lumen and the muscular walls of the blood vessels. This means that this can be used to directly see clot or plaque within the walls of the blood vessel.

Figure 4. MR angiography showing from aortic arch to circle of Willis.

The application of MRA for different regions of the human body has evolved rapidly over the years. In the head and neck region, MRA is useful for evaluating flow in the carotid arteries, the circle of Willis (see Figure 4), the anterior, middle, and posterior cerebral arteries, the vertebral, basilar arteries, and the venous sinuses. MRA is useful in patients for whom surgery is anticipated and those conditions include tumours, aneurysms, vascular malfunctions, and vascular occlusions or thrombosis. MRA is also useful in determining the presence and extent of peripheral arterial vascular diseases of the lower extremities. It has been shown to be useful for detecting occult vessels. It is also a good diagnostic tool for pre-operative evolution in patients of elective abdominal aortic aneurysm (AAA) repair. MRA determines the extent of the AAA as well as the extent of aortoiliac occlusive disease and renal artery pathology that is required in planning for the AAA repair. MRA has also been shown to be useful in many cardiac abnormalities[15]. Recently contrast enhanced (CE) MRA has emerged as a new tool, which is advantageous in situations of tortuous vessels and stenotic regions. Due to the fact that Gd-DTPA has no nephrotoxic potential, its use in kidney studies is widely accepted. Depiction of large aneurysms is markedly simplified with CE-MRA compared to DSA. The main advantage of CE-MRA compared to TOF and PC MRA is its intrinsic advantage in acquisition speed.

Diffusion and perfusion MRI

Recently, the ability of MRI to image and measure molecular diffusion and blood microcirculation (perfusion) has become an important tool. Diffusion and perfusion imaging[16,17] is useful in the evaluation of anatomic and functional disorders of the brain and other organs. Both methods share some conceptual points but however, refer to different physical phenomena. Molecular diffusion is the result of the thermal, so-called Brownian, random translational motion that involves all molecules, while perfusion is related to blood delivery to tissues.

Diffusion-weighted MR imaging (DWMRI or DWI) is used to map as well as assess and/or quantitate the microscopic motion of water protons in tissues[16,17]. Measurement of molecular diffusion may lead to several potentially useful new approaches of tissue characterization and functional studies. Data of DW images are presented in many ways: as DWIs, T2-corrected DWIs, and apparent diffusion coefficients (ADC) and as ADC maps. In clinical imaging, however, diffusion is defined by ADC. In tissues, water interactions and collisions with macromolecules and membranes usually limit diffusion.

In brain, the signal intensity on DWI depends primarily on the ability of water molecules to move within and between the intracellular and extracellular spaces via permeable cell membranes. Thus, the local environment influences diffusion; for example, in areas of white matter there is greater diffusion along the myelin sheaths than across them. Therefore, the diffusion of water in tissues is anisotropic; i.e. there are different ADCs in each direction. In fact, diffusion is a three-dimensional process and the molecular mobility may not be the same in all directions. This anisotropy results from the physical arrangement of the medium or from asymmetric disposition of obstacles that limit diffusion. In fact, diffusion is a tensor, an array of numbers that describe mobility rates in different directions. Diagonal elements D_{xx}, D_{yy}, and D_{zz} represent molecular mobility in the three directions X, Y, and Z-axis. The non-diagonal elements, such as D_{xy}, D_{xz}, or D_{yz}, show how diffusion in one direction is correlated with some molecular displacements in a perpendicular direction. Molecules can diffuse in all three dimensions and hence diffusion tensor mapping becomes more useful. Diffusion is a major advance in the continuing evolution of MR imaging. It provides contrasts and characterization between tissues at cellular level that may imply differences in function[16,18].

DWI is useful in the early detection and characterization of cerebral ischaemia and renders this technique ideal for evaluation of stroke management[16,19,20]. Figure 5 shows our data on diffusion-weighted image of a patient who was subjected to MRI investigation 6 h after the onset of ischaemia. The infarct region is seen clearly as a hyperintense area, which could not be clearly differentiated in the T2-weighted image. DWI technique allows more efficient and accurate measurement of stroke volume in experimental animal models[21–23] (vide infra). Recently we have documented through sequential DWI study; the occurrence of several pathological features during acute as well as during the complete cycle of demyelination and remyelination in an animal model with demyelinating lesion[24].

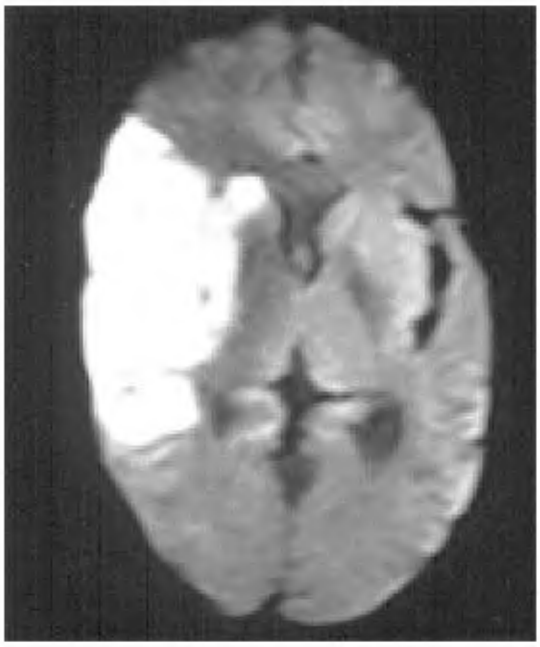

Figure 5. Diffusion-weighted MR image of a patient investigated 6 h after ischaemic stroke. The infarct region in seen clearly as hyperintense area in the right occipital region.

Diffusion tensor images and fractional anisotropy (FA) maps are useful to predict the directionality of white matter tracts. This is called as 'diffusion tractography', which can be used to identify specific white matter tracts, not just white matter tracts in general. For example, the location of the corticospinal tract or the thalamocortical tract can be determined and these tracts can be differentiated from all the other white matter tracts in the corona radiata. Such informations have impact on the treatment of lesions in the brain. Recently, high b value DW imaging has also been evaluated to differentiate tumour sub-types.

Perfusion MRI (PWI) measures blood flow, which is different in many brain and cardiac disorders[16,25]. In fact, perfusion MR demonstrates the microscopic vascular proliferation (neovascularization) associated with tumour growth. Tissue perfusion is normally assessed following a dynamic injection of contrast material like gadolinium diethylene triamine pentaacetic acid (Gd DTPA). For example in cerebral tissues, Gd is restricted to the intravascular space. Gd being paramagnetic creates microscopic field gradients around the cerebral microvasculature, resulting in a change of T2 relaxation and signal loss. From the amount of signal loss, the concentration of gadolinium in each pixel can be calculated, and a pixel by pixel relative estimate of blood volume can be inferred. Maps of cerebral blood volume (CBV) and cerebral blood flow (CBF) can be generated. High-grade tumours have higher CBV values than low-grade tumours and CBV values correlate with the grade of vascularity and mitotic activity. Knowledge of tumour vascularity is helpful to improve tumour grading, to identify optimal biopsy site in tumours with heterogeneous vascularity, to monitor for malignant degeneration and treatment efficacy, and to differentiate tumour recurrence from radiation necrosis. Similarly, PWI of myocardium is a useful modality to detect perfusion defects at rest and under stress. Contrast enhanced (Gd DTPA) PWI can be reliably used for assessment of myocardial perfusion in patients with ischaemic or infarcted myocardium. The uptake of contrast will be attenuated, in amplitude and rate, in regions of compromised flow.

Functional MRI

Another advance in MRI is to map changes in brain haemodynamics that correspond to brain functions known as functional magnetic resonance imaging (fMRI). This

technique has been evolving as one of the most powerful noninvasive techniques to map the areas of neuronal activation in human brain during sensory/motor task[26–31]. In 1990, it was discovered that the intensity of MR signal in the vicinity of veins and in brain parenchyma was reduced with decrease in blood oxygenation[26,32]. This contrast mechanism known as blood oxygenation level dependent (BOLD)[27] forms the basis of noninvasive imaging modality to monitor several cognitive functions. fMRI can be used to detect increased cerebral blood volume[33], flow[34] and blood oxygenation[35,36] that occur in association with increased neuronal activity during activation.

The basis of fMRI is that the deoxy haemoglobin present in blood is a paramagnetic substance, which in the presence of an external magnetic field alters the magnetic field in its vicinity[27]. This affects the magnetic resonance behaviour of water protons within the surrounding vessels resulting in an observable change in the image intensity. An increase in neuronal activation by a stimulus or task lead to an increase in the arterial blood flow without a commensurate increase in oxygen extraction that results in proportionate decrease in venous deoxy-haemoglobin concentrations in capillaries[37]. This manifests as an increase of the relaxation parameters T2* and T2 and consequently an increase as signal intensity in T2* and T2 weighted MR images, the so-called BOLD effect[27].

fMR activation images can be superimposed on high-resolution anatomical images that aid the specification of the positions of activity foci within the brain. Several applications of fMRI in identifying brain regions activated during word generation, visual processing, speech perception, working memory and spatial memory have been documented. In addition, organizational differences related to handedness[38] and focal activity[39] have been demonstrated. Figure 6 shows the multislice BOLD fMR images of a normal subject performing simple finger movement of the both hands simultaneously. The cortical activation in both the hemispheres of the brain is clearly seen.

fMRI has been extensively used to map the primary motor cortex locations for fingers, toes, elbows and tongue[29,38,40]. It is successfully applied for preoperative localization of the sensory motor cortex and its relationship to a mass and also to predict postoperative functional deficits. Several investigators have documented the utility of fMRI to map language centres in the brain[41–43]. It is used to demonstrate that language could be lateralized during internal speech word generation[42]. Bilateral activation of the superior temporal gyri during passive word listening has also been demonstrated[44].

Studies reveal that women on average have slightly better verbal skills than men[45,46]. Activations in men are significantly more left lateralized than in women across the cortex during both phonologic and semantic tasks. fMRI has also been widely used to study the retinotopic organization of the primary visual cortex[47,48], visual motion[48] and cognitive aspects of visual perception such as pathways involved in relation to face identity[49]. Post-ejaculatory refractive period (PERP) is a state of active sexual inhibition during which any intensity of sexual stimuli is unable to elicit any sexual arousal in the male[50]. Functional MR imaging of brain was carried out to localize the brain areas involved in PERP in young healthy males[51].

Identification of epileptic zone and assessment of memory functions of epileptic patients has been studied using fMRI[39,52,53]. Determination of the precise location of seizure origin is important for successful surgery to avoid associated postoperative morbidity. Direct localization of the cerebral origin of seizures in patients with intractable seizures is possible with fMRI[52–54]. After identifying the epileptic zone, fMR images facilitate the clinician to localize the expressive cortex and its relationship to the epileptogenic zone prior to operation.

fMRI has immense potential for studying brain in various psychiatric disorders like anxiety, depression, attention deficit, hyperactivity disorder and schizophrenia. Schizophrenic patients demonstrated an overall diminished response to motor tasks; however, the involvement of primary motor cortex or supplementary motor area (SMA) is not established in schizophrenia[55–57]. A reduced activation within auditory cortex has been found in schizophrenic

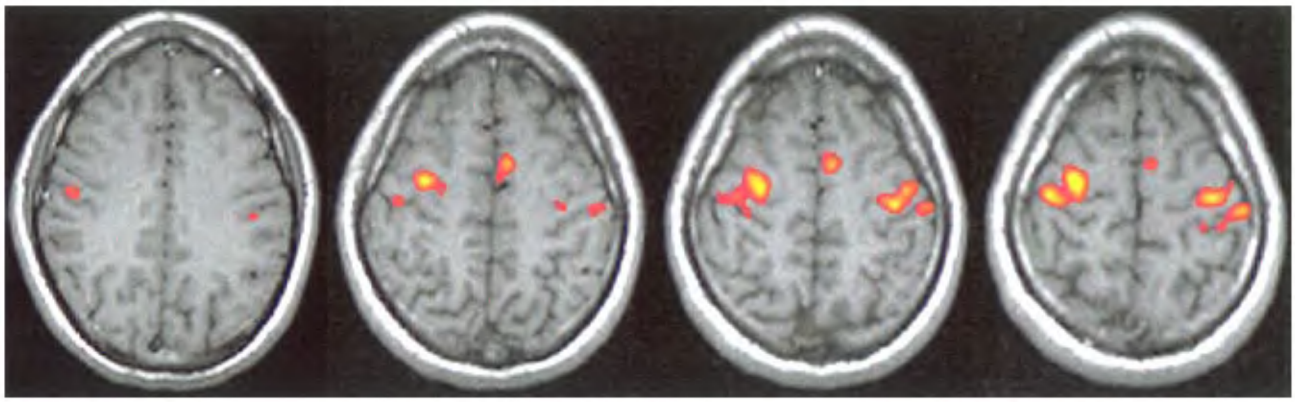

Figure 6. Functional MR image of a volunteer carrying out finger movements of the both the hands simultaneously. The appropriate cortical activity in the left and right motor area in different slices is shown as hyper-intense signal on a T1-weighed axial MR image.

patients with auditory hallucination. Recently, fMRI has also been used to investigate the part of the brain that manages our perception of time. Such studies would lead to new drugs for patients with Parkinson's disease, who often experience problems with time perception. fMRI has an important role in pain management and holds great promise for unravelling the neuro-anatomic basis of many psychiatric diseases.

MRI of nuclei other than protons

In recent years there has been considerable interest in MR imaging of nuclei other than proton such as ^{23}Na and ^{19}F. Such measurements are exacerbated by the low intrinsic sensitivity of these nuclei relative to proton and the low physiological concentrations relative to water. Sodium MRI studies have demonstrated that the method can be useful for monitoring oedema development, cerebral redistribution of sodium following ischaemia[58] and myocardial infarction[59]. It is a useful technique to detect early cartilage degeneration[60]. Since there is no MR visible fluorine in human body, the ^{19}F MRI methodology depends on the exogenous addition of a fluorinated material. Perfluorocarbons that label vascular compartments at high concentration have been commonly used, especially in the assessment of vascularity and the kinetics of tissue perfusion[61].

Recently, studies have shown that inhalation of hyperpolarized (HP) gas allows images of the human lung air spaces by MRI with excellent contrast resolution[62–67] since conventional proton MRI yields very poor images of the lungs because they are filled with air and contain little water. Gases like is ^{3}He or ^{129}Xe, both chemically inert noble gases with spin 1/2; are polarized by optical pumping before inhalation. Nuclear polarization up to 80% is achieved which corresponds to a huge polarization enhancement or hyperpolarization above the thermal polarizations obtained in standard MRI. This method has applications in the domain of lung pathology and other perspectives in functional MRI.

Pharmaceutical applications of MRI

The application of MRI in pharmaceutical research like study of the efficacy of drugs and pharmacokinetics of drugs enables us to understand the pathophysiology of interaction of drugs with the tissues *in vivo*. The method also allows *in vivo* drug concentration determination in tissues. MRI has been used to investigate the early pathological events associated with cerebral infarction in animal model such as unilateral occlusion of the common carotid artery in gerbils[68] or the middle cerebral artery occlusion (MCAo) in animals[7]. The MCAo model in rats has been used to test drugs with various mechanisms, aimed at reducing the extent of cellular damage in the acute phase of stroke. These drugs are calcium antagonists, NMDA antagonists, AMPA antagonists, ion channel modulators, anti-inflammatory drugs, etc. In several cases it was demonstrated that the cytoprotective effects found at 24 or 48 h after MCAo persisted up to 14 and 28 days and could in these cases be considered permanent[69,70]. Several drugs also showed efficacy when administered after permanent MCAo[71].

Progression of a focal ischaemic lesion in rat brain during treatment with a novel glycine/NMDA antagonist was studied by *in vivo* 3D diffusion weighted MR[21]. It was documented that the stroke volume increased by 15% in the control group, in contrast to the treated group that showed a 40% reduced stroke volume. Of the several mechanisms of neuronal injury in stroke, free radicals have also been implicated during ischaemic re-perfusion. Melatonin, a potent antioxidant, has been used in male Wistar rats subjected to 2 h of transient middle cerebral artery occlusion (MCAo) to study the effect on ischaemia[22]. Melatonin (10, 20 and 40 mg/kg i.p.) was administered four times to the animal at the time of MCAo, 1 h after MCAo, at the time of re-perfusion and 1 h after re-perfusion. In the 20 mg/kg melatonin tested group, per cent ischaemic volume in DWI was significantly attenuated compared to the vehicle treated group (Figure 7).

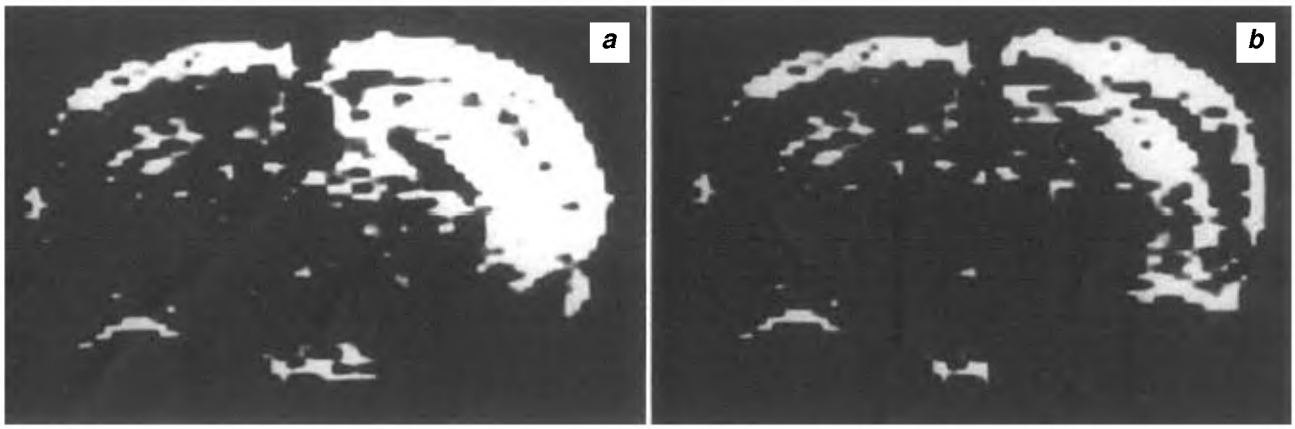

Figure 7. ***a***, DW image of vehicle-treated middle cerebral artery-occluded rat, 30 min after reperfusion; ***b***, DWI of melatonin-treated rat 30 min after reperfusion.

The study indicated that melatonin has neuroprotective action in focal ischaemia, which may be attributed to its antioxidant property[22]. Similarly, the effectiveness of adenosine as a neuroprotective agent in MCA occluded rats using DWI has also been demonstrated[23].

Contrast enhanced dynamic MRI was used to investigate the diltiazem-induced microcirculatory changes in tumour and normal muscle of Swiss albino stain A mice[72]. In addition, the MR BOLD contrast method was also used to assess tumour oxygenation status before and after diltiazem administration. The diltiazem plus radiation-treated mice showed significant tumour regression and enhanced animal survival. Thus, the study revealed that diltiazem has the potential as an adjuvant in radiation therapy apart from its use in chemotherapeutic drug delivery[72].

In modern drug discovery and development, transgenic and knockout animals are of importance as disease models and for target validation. Several examples of MRI and MRS applications in this field have also been reported[73,74]. The well-studied system is the creatine kinase, which plays a critical role in the high-energy phosphate (HEP) metabolism[74]. In transgenic animals with increased expression of creatine kinase in skeletal muscle, no changes in the steady-state HEP levels have been observed, despite increased contractile function.

Interventional/intraoperative MR imaging

With the introduction of open magnet designs offering a nearly free patient access, interest has now focused on interventional MR[75]. The concept of intraoperative/interventional MRI is related to the idea of minimal invasiveness. However, the requirements for intraoperative/interventional MRI are more complicated than the diagnostic imaging. Percutaneous biopsies and drainage procedures are currently the easiest procedures to be performed under MR. These do not require dedicated hardware- or software modifications and are thus attractive and clinically useful. Improved patient access with open magnet allows interventions in any desired plane and patient position. In closed systems, instrument manipulation can only be performed with the patient outside the magnet. However, due to higher field strength, image quality as well as the imaging speed is better.

In MRI-guided biopsy, biopsy needles are displayed as dark areas surrounded by a brighter rim. Several vendors offer MR compatible needles. Fine needles of varying size with different tip configurations and cutting needles are commercially available. For drainage procedures MR compatible sets consisting of MR compatible guidewires, dilators and drainage catheters are also available[75].

The methodology consists localizer images in three planes followed by a fast multislice T2W images. A post-contrast fast gradient-echo sequence may be used to select the appropriate biopsy site. In the closed magnet, needle tracking is done following a procedure similar to that used in CT-guided intervention. After defining the target region, a T1W or T2W compatible grid is fixed to the skin of the patient to aid in selecting needle entry site. The angle and distance from skin to the lesion can be obtained by using standard scanner software. The needle track can be controlled step-by-step during advancement of the needle. In the open magnet, a palpating finger may be used instead of a grid for entry site. The instrument can be tracked by continuous repetition of a fast imaging sequence.

Primary and secondary bone and soft-tissue lesions, intra-cranial lesions, neck tumours, etc. can be accessed by MR-guided interventional procedures. Due to multiplanar capability, MR allows visualization of the entire planned biopsy pathway including orthogonal and oblique scans. Deeply embedded soft tissue lesions would obviously be more amenable to MR guidance rather than CT or ultrasound. The use of MR for intervention however, may be limited by the size of the lesion, as lesions smaller than 1 cm may be obscured by the artifact caused by the needle, and the needle tip cannot be documented to be within the target. MR interventions have the potential to enable temperature monitoring, which introduces opportunity to use MR guidance for thermal (laser) ablation or cryoablation of lesions.

In vivo MR spectroscopy

In vivo MRS is carried out with nuclei that have high natural abundance and sensitivity in living systems. For these reasons, most of the applications of *in vivo* MRS have been using ^{1}H and ^{31}P nuclei[6–8,10–12]. In living systems, there are two main sources of protons namely water and fat that are used for image formation in MRI. However, the protons of water and fat mask the signals of metabolites that are present in low concentration in tissues. Therefore, the detection of resonances of biochemicals with low concentration requires suppression of the water signal[76–78].

Localized MRS

The aim of *in vivo* MRS is to obtain a spectrum that arises exclusively from the voxel of interest (VOI), with the best achievable sensitivity and with minimum contribution from other regions. There are different localization techniques available in clinical use today. Magnetic field gradients in either the $\mathbf{B_0}$ field as in imaging or in the $\mathbf{B_1}$ (RF) field are used for localization of a particular volume. In general, MRS requires a homogeneous $\mathbf{B_0}$ field for signal acquisition. One of the earliest methods for localization of VOI is to employ surface coils. The early localization methods like rotating frame spectro-

scopy uses $\mathbf{B_1}$ field of the surface coil for localization. Methods like depth resolved spectroscopy (DRESS) use $\mathbf{B_0}$ magnetic field gradients and a frequency selective pulse for localization. The commonly employed sequences include stimulated acquisition mode (STEAM), point resolved spectroscopy (PRESS) and image guided *in vivo* spectroscopy (ISIS). Currently multivoxel spectroscopic [chemical shift imaging (CSI) or spectroscopic imaging (SI)] methods are also available which are used to acquire spectra from many voxels, simultaneously. Since most of these methods use MR images to guide the VOI localization, they are often termed as image-guided localization methods.

Single voxel MRS: Stimulated echo acquisition mode (STEAM) uses three frequency selective RF pulses that are applied in succession in the presence of mutually orthogonal *x*, *y* and *z*-field gradients[79,80]. The localized VOI is at the intersection of the three orthogonal slices. Each pulse is of 90°, and also since the pulse angle can be less than 90°, the RF power deposition on tissues is less. Due to high quality localization obtained with STEAM, it is one of the most frequently used single voxel MRS techniques despite the disadvantage that there is loss of a factor of two in S/N compared to Curr–Purcell echoes. STEAM is not well suited for observation of nuclei with short T2 values like ^{31}P. In general, the T2 for protons are much longer than the T2 of ^{31}P, and the use of STEAM has been primarily for localized proton MRS.

The point resolved spectroscopy (PRESS) or double spin-echo[81,82] offers the important advantage of a factor of two gain in S/N, although signals are T2 weighted and J-modulated. The VOI definition and localization in PRESS is inferior to STEAM since the slice profiles of the 180° pulses are often worse than those of a 90° pulse. Further, the power requirement for 180° pulses is twice that of a 90° pulse, which may cause RF heating of tissues. Another disadvantage is the lengthened minimum echo time that is an important limitation for metabolites with short T2.

Multi voxel MRS: Single voxel ^{1}H NMR spectroscopy can be extended to multivoxels called chemical shift imaging (CSI) or spectroscopic imaging (SI)[83,84]. Since localized spectra from many locations can be acquired simultaneously, SI is a more attractive method than single voxel techniques. Figure 8 *a* shows the coronal MR image of a patient suffering from glioma wherein the CSI or the VOI grid is shown as a big square while Figure 8 *b* is the proton MR spectrum obtained from one of the voxels (shown by arrow) of CSI from the tumour region. Figure 9 *b* shows the proton spectrum obtained from one of the voxels from the normal portion of the tissue as shown in Figure 9 *a* of the same patient. The advantages of SI include acquisition of spectral data from small VOIs and the ability to reconstruct low-resolution metabolite images from the spectral data in which the pixel intensity is proportional to the relative concentrations of the metabolites. These metabolic maps or images are useful in visually assessing the spatial variation in the metabolite concentrations. EPI-based SI sequences are now available, which decrease image acquisition times.

Recently hybrid SV-SI pulse sequences that combined STEAM SI localization of a large volume of interest has been developed. Here, the advantage of SI localization from multiple voxels is retained, while the use of the SV method to preselect the large VOI greatly minimizes

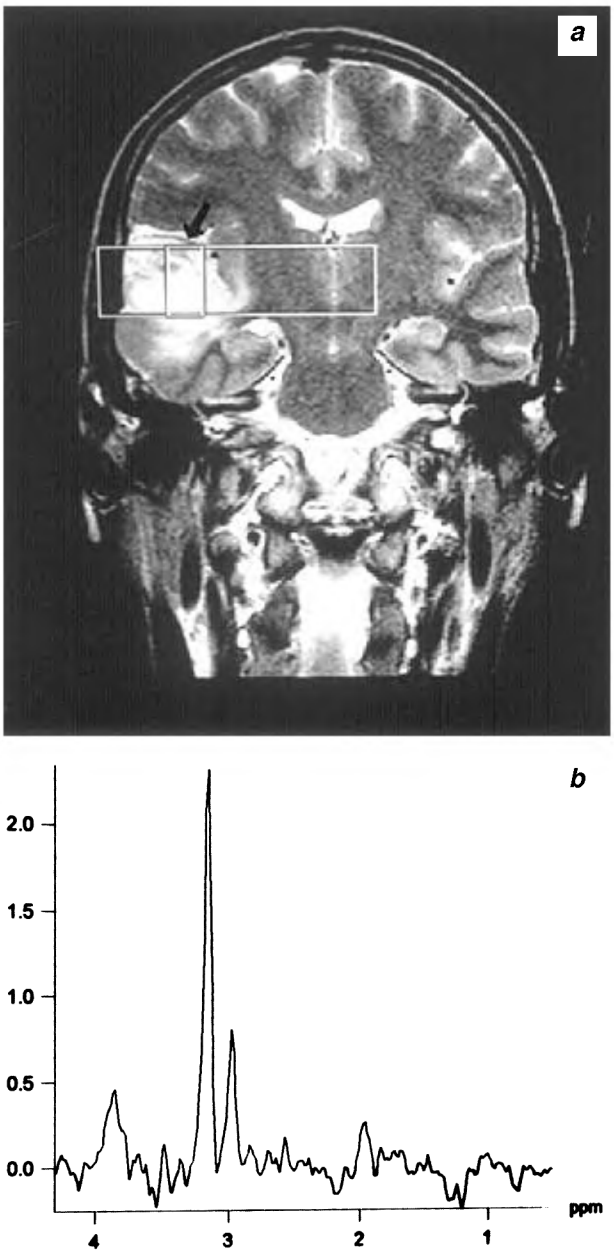

Figure 8. *a*, T1-weighted coronal brain image of a patient with glioma. The CSI grid is the bigger rectangle which is divided into several small voxels from which proton MR spectra are obtained; *b*, Proton MR spectrum from a voxel (shown by arrow) which is located inside the rectangular grid.

spectral bleed contamination from the outside lipid signals. The method allowed improved shimming, improved spectral resolution and water suppression. Several multidimensional experiments have demonstrated the potential of SI in the study of human brain[85–88].

Clinical applications of in vivo MRS

Over the past decade *in vivo* MRS has increasingly been applied in clinical setup using nuclei like ^{1}H and ^{31}P to study the metabolism of several disease processes. A brief overview with some examples from our own study and from the literature is presented here.

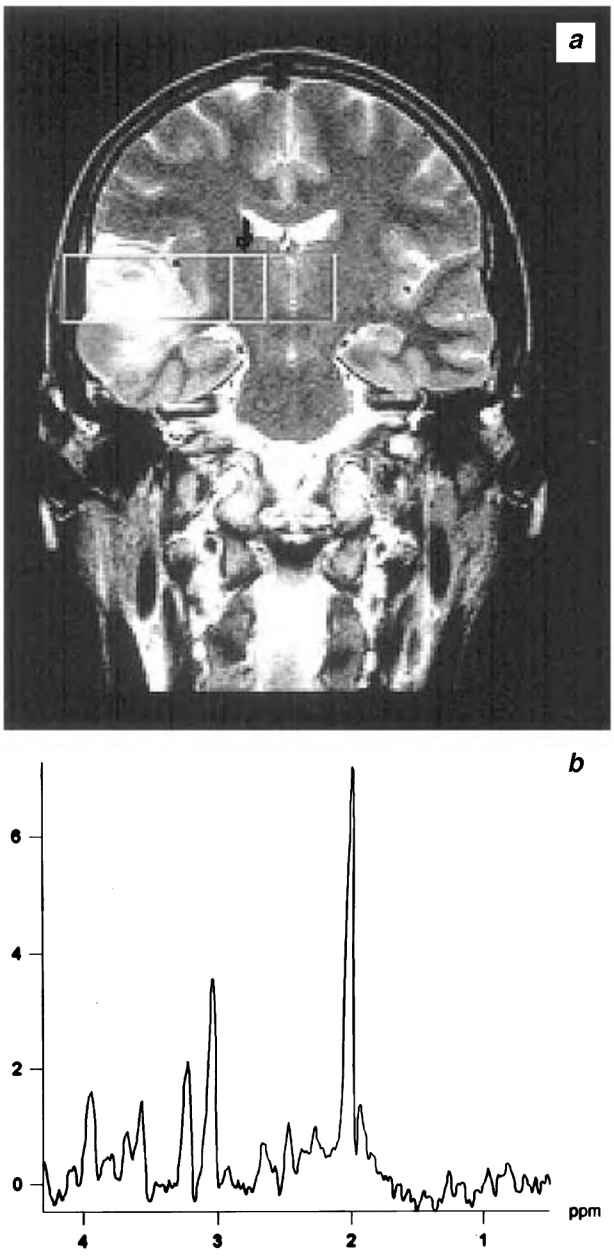

Figure 9. *a*, T1-weighted coronal brain image of the same patient shown in Figure 8; *b*, Proton MR spectrum from a voxel (shown by arrow) which is shifted away from the tumour site (normal portion of the tissue).

Phosphorus MRS: ^{31}P is the naturally occurring nuclei that has been most extensively used for studying *in vivo* tissue energetics. The spectra are simple since the MR signals are observed only from the relatively mobile compounds, which are in mM concentration. Thus, monitoring the relative concentration of various ^{31}P metabolites noninvasively helps to study the biochemistry of diseased and normal states of tissues and can also be used to monitor the efficacy of several therapeutic interventions. Figure 10 shows the ^{31}P MR spectrum from the human calf muscle of a volunteer recorded in our laboratory. The spectrum shows resonances from β-adenosine-tri-phosphate (ATP), at – 16 ppm, signal at – 2.5 ppm is characteristic of γ-ATP while the signal at – 7.5 ppm contains contributions from the α-phosphate groups of both ATP and adenosine-di-phosphate (ADP). The resonances at 0 and 5 ppm are due to phosphocreatine (PCr) and inorganic phosphate (Pi) respectively.

The chemical shift position of Pi is sensitive to pH and provides a noninvasive indicator of intracellular pH. Besides Pi, ATP and PCr, signals from phosphomonoesters (PME; 6–8 ppm) and phosphodiesters (PDE; 2–4 ppm) are also observed. The PME peak contains several compounds such as sugar phosphates and phosphocholine (PC). The metabolic state of cells can thus be studied by monitoring the PME peak. Increase in PME in malignant cells suggests alterations in lipid metabolism[89,90]. Glycerophosphocholine (GPC) and phosphoethanol amines (PE) are major PDE components observed in ^{31}P spectra. The chemical shift positions of the β and γ phosphates can also

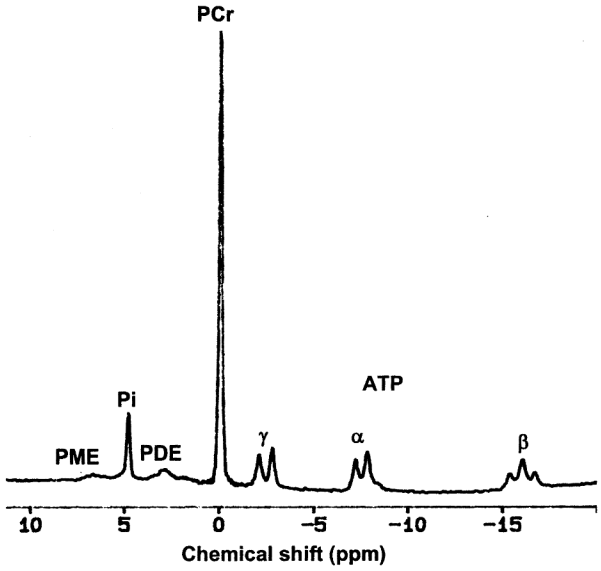

Figure 10. ^{31}P MR spectrum from the calf muscle of a normal volunteer recorded using a surface coil with single pulse technique with a repetition time of 3 s.

be used to obtain information whether ATP is complexed to divalent metal ions like Mg^{2+}.

The ^{31}P spectra of brain of normal newborn human infants showed high PME[91,92] and decreased PME/PDE ratio during the first six months of life with a significant increase in PCr/ATP and variation in NAD[93]. Significant differences between normal and brain tumour tissues have been reported. Reduction in PCr and PDE with increased PME are observed in meningiomas, while malignant gliomas showed less distinct changes[94]. In meningiomas, alkaline pH and decrease in PCr and PDE metabolites was noticed. Glioblastomas also showed alkalization and a decrease in PDE/α-NTP but no significant changes in PCr/α-NTP or PCr/Pi ratios. In low-grade gliomas, less distinct changes were detected with slight alkalization and more than a two-fold reduction in the PDE/α-NTP ratio.

The changes in muscle metabolism at rest, during exercise and recovery has been extensively studied by sequential ^{31}P MRS. In normal exercising muscle the concentration of ATP remains constant while PCr falls, and that of Pi is increased[95]. Intense exercise produces severe intracellular acidosis (pH < 6) and acute changes in muscle pH, presumably reflecting a balance between early proton consumption by PCr hydrolysis and lactate production by glycolysis[95]. During recovery PCr gradually increases while Pi and ADP decreases, and the pH returns to its rest level. The effect of aging on muscle metabolism has been reported and that PCr/(PCr + Pi) and pH at rest and after the completion of the exercise did not differ between young and older subjects[96]. In chronic malnutrition, the level of PCr/ATP at rest in the muscle is reported to be reduced[97,98].

^{31}P MRS investigations of various neuromuscular and mitochondrial diseases have also been reported[95,99,100]. The level of PCr/Pi at rest was reported to be abnormally low in mitochondrial myopathy[95]. Furthermore, ^{31}P MRS is also useful in discriminating disorders of glycogenolysis (McArdle's disease) and glycolysis[95]. A high intracellular pH and reduction in the level of PCr at rest has also been reported in the muscle of patients with muscular dystrophy[92,95]. In patients with Becker's dystrophy[101–103] and carriers[102,103], during exercise a premature drop in PCr levels (or PCr/Pi) and reduced acidosis was reported.

Several studies have been reported on the normal and breast cancer tissues[94,104,105]. In the normal breast tissue PME was lower, while the PDE/PME ratio was higher during the second week than at the other stages of the menstrual cycle. PME was also seen to be increased in the lactating breast by a factor of two compared to the non-lactating premenstrual breast[94].

Proton (^1H) MR spectroscopy: Proton MRS has been widely used to study the tissue metabolism due to its high sensitivity, 100% natural abundance and its presence in all biologically important metabolites. However, there are major technical problems associated with ^1H MRS since there is a need to suppress water signal, which are several hundred times higher in magnitude than the metabolites of interest. With the development of techniques of water suppression and spectral editing, ^1H MRS is now being routinely employed to study the biochemistry of brain, muscle, breast and other organs.

The proton MR spectrum recorded from the fronto-parietal region of the brain of a normal volunteer is shown in Figure 11. The peak at 2.02 ppm corresponds to *N*-acetyl group of the amino acid *N*-acetyl aspartate (NAA) and is evenly distributed throughout the cerebral cortex. A small fraction of *N*-acetyl aspartyl-glutamate (NAAG), a neuromodulator or neurotransmitter also contributes to this signal. As per the prevailing concept, NAA is considered as a neuronal marker of oligodendrocyte precursor[106,107]. Non-cerebral tumours show little or no NAA. The concentration of NAA is reduced in diseases like hypoxia, ischaemia, dementia, Alzheimer's, epilepsy, MS, stroke, neoplasm, lymphoma and tumour.

The *N*-methyl protons of creatine and phosphocreatine (Cr/PCr) appear as a strong peak at 3.02 ppm. Minor contributions to the intensity of this peak may come from GABA, lysine and glutathione. The peak from $N–CH_2$ of Cr resonates at 3.94 ppm. Although Cr is of little biochemical interest, the equilibrium enzyme creatine kinase (conversion of Cr to PCr) appears to be crucial to the maintenance of energy-dependent systems in all the brain cells. Cr also functions as an osmolyte responding to osmotic (Donnan) forces. Thus, Cr is increased in hypermetabolic and hyperosmolar states and decreased in stroke, toxoplasmosis, PML, tumour and hyponatremia[108].

The choline metabolite observed in the brain spectrum is from the N (CH_3) protons which exhibit a strong signal at 3.22 ppm and has contributions from other choline containing compound such as GPC, PC and PCho. These are components of phospholipid metabolism of cell membranes and hence increased Cho may reflect increased membrane synthesis. Cho is also involved in the synthesis of neurotransmitter acetylcholine and phospholipids. Cho level increases in many solid tumours and high-grade solid gliomas generally have higher Cho than low-grade solid tumours. The level is also increased in diabetes, neonates, post-liver transplant, chronic hypoxia and stroke. In asymptomatic liver disease, hepatic encephalopathy (HE), toxoplasmosis, nonspecific dementia and hyponatremia, the Cho levels have been found to be decreased.

The concentration of Lac is very less in the normal brain and its presence therefore, suggests that normal cellular oxidative respiration mechanism is no longer in effect and energy is derived via anaerobic glycolytic activity. The methyl protons of Lac appear as a doublet at 1.33 ppm and are increased in hypoxia, anoxia, near drowning, stroke, Canavan's, Alexander's, lymphoma and toxoplasmosis.

Resonances due to Glu and Gln appear as broad peaks between 2.1 and 2.5 ppm in the *in vivo* ^{1}H MR spectrum and are normally detected at short TE. Glu is the most abundant of the amino acids in the brain and acts as excitatory neurotransmitter. Gln is probably important in the detoxification and regulation of neurotransmitter activitiy of its precursor Glu; while GABA is an inhibitory neurotransmitter. In various neurologic disorders such as cerebral stroke, prolonged seizures, neurodegenerative disorders, hypoglycaemia and mitochondrial encephalopathy, a disturbance of the normal Glu–Gln regulatory metabolism has been suggested to be present[109].

Myo-inositol (mI) appears at 3.56 ppm, is a control metabolite in neural function and has been suggested as a possible degradation product of myelin and a marker of glial cells. mI has been found to be increased in patients with Alzheimer's[110], diabetes[10,11] and HE[10,11]. In addition, resonances due to glucose (Glc; at 3.43 and 3.50 ppm) can also be observed. The direct observation of Glc however, is hampered by the water signal as well as due to the overlap with taurine, mI, Glu and Gln resonances. Resonances due to lipids are observed at 0.8, 1.2, 1.5 and 5.3 ppm which are due to the methyl, methylene, allelic vinyl protons of the unsaturated fatty acids. Membrane lipids generally have very short relaxation times in brain and are not normally observed at long TEs. Lipids may be increased in high-grade astrocytomas and meningiomas and may reflect necrotic processes.

^{1}H MRS has been extensively used in evaluating several brain pathologies[10,11,111–113]. Typical proton MRS characteristics of astrocytoma are significant reduction in NAA, elevation in Cho and modest reduction in Cr. Figure 12 is the proton MR spectrum from a 8 ml voxel positioned in the tumour (Figure 12 *a*) of a patient suffering from mixed glioma. Figure 12 *b* and *c* were recorded at an echo time (TE) of 135 and 30 ms respectively, showing the high level of Cho and the presence of Lac with reduced Cr and NAA. Proton MRS also plays a crucial role in monitoring the response to treatment of disease processes and differentiating the recurrence of tumours from post-treatment effects. It has been used in differentiating high-grade gliomas from metastases[114]. The potential indications of the clinical application of ^{1}H MRS are pressurized tumour grading, early detection of anaplastic transformation and monitoring treatment procedures[115].

Increase in Cho is also observed in meningiomas[116] with sometimes elevated Lac and Ala also. Lymphomas show elevated Cho and lipids with reduction in Cr and NAA. *In vivo* proton MRS on patients with malignant glioma before and after radiotherapy treatment and surgery has been reported[117]. In case of hyperacute stroke the first visible change in the ^{1}H MRS after the onset of ischaemia is the appearance of lactate. Decreased NAA can be seen within 30 to 60 min of induced cerebral infarction. Changes in Cho and Cr concentration during acute infarction seem to be more variable than changes in Lac and NAA. Graham *et al.* reported that macromolecule signals were elevated in stroke relative to normal brain and tend to increase in the subacute period even as Lac peak declined[118]. Elevated Lac levels without changes in NAA or Cho suggest the area of ischaemic penumbra. Recently, using diffusion imaging and MR spectroscopy it was

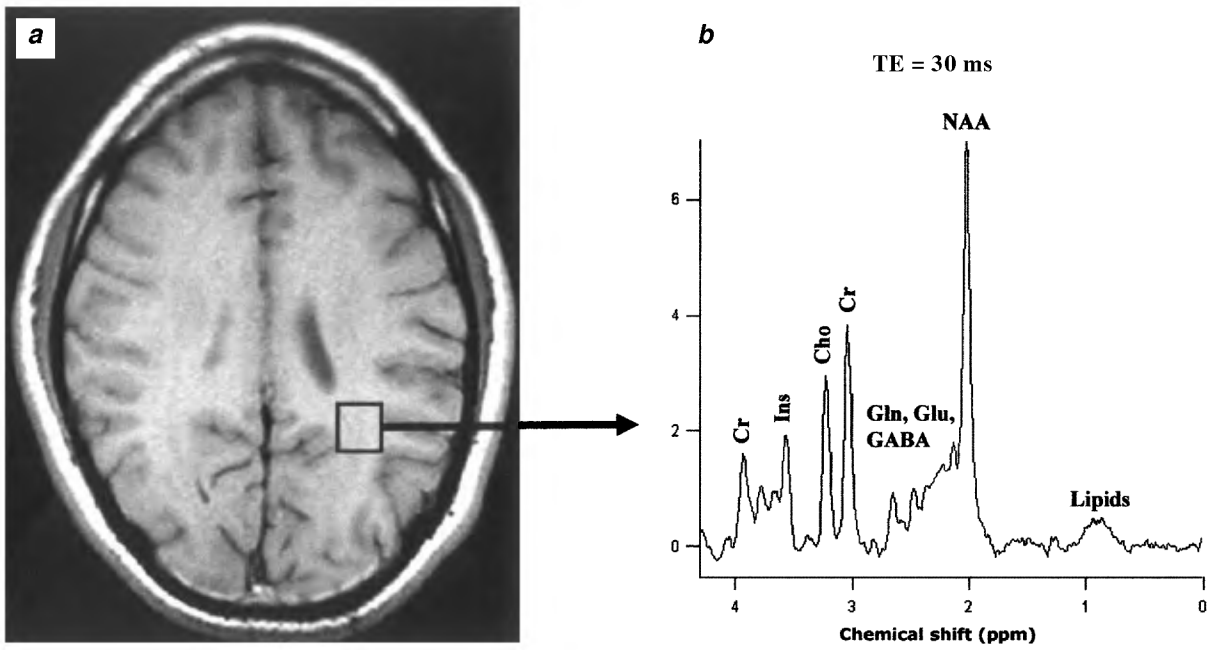

Figure 11. Water suppressed proton MR spectrum from an 20 × 20 × 20 mm^3 voxel acquired from the fronto-parietal region of the brain of a volunteer obtained using PRESS pulse sequence at an echo time (TE) of 30 ms with a repetition time (TR) of 3 s and the number of averages accumulated = 256.

shown that both ADC and Cho are related to glioma cell density[119]. Intracranial lesions, tuberculomas, neurocysticercosis and nonspecific inflammatory lesions showed significant differences in NAA/Cr, and Cr/Cho ratios. Lipids were seen in 86% of tuberculomas[120].

In vivo proton MRS is also useful in many disease processes where molecular level changes occur much earlier than structural changes. Using ^{1}H MRS the effect of alcoholism in frontal lobe, cerebellum and thalamus regions of brain in alcoholic patients was studied[121]. The MR images of these patients revealed no structural changes, however, the proton spectra were characterized by a reduced NAA/Cho and NAA/Cr ratios relative to age matched controls. Reduction in NAA was consistent with neuronal loss while reduction in Cho is suggestive of significant changes in the membrane lipids of alcoholics. Similarly, reversal of abnormalities of myelination by thyroxine therapy in congenital hypothyroidism was also demonstrated by using proton MRS while MR imaging revealed no abnormality. Biochemical changes in different regions of brain in congenital hypothyroidism before and after thyroxine therapy was documented using *in vivo* ^{1}H MRS[122]. An abnormal lipid peak that disappeared with thyroxine therapy was observed in cerebellum and frontal lobe in one patient. Significant reduction of NAA/Cr and elevation of Cho/Cr ratios in comparison to controls were documented in these patients, which tended to normalize with thyroxine therapy[122].

Cerebral biochemistry in several neuropsychiatric disorders has also been reported[123,124]. Reduced NAA in the temporal and cerebellar regions has been reported in individuals with autism[123,124]. NAA in the thalamic region was significantly reduced in schizophrenic patients, whereas Cho and mI were significantly increased in parietal white matter[125]. In the study of neurodegenerative diseases in older adults like Alzheimer's, a decrease in NAA and elevated levels of mI and Cho have been reported[123,124]. Biochemical changes associated with seizures and epilepsies report decrease in NAA and NAA/Cr ratio, while in some cases only low concentration of NAA and no changes in the levels of Cr and Cho was observed. Increase in Cr, Cho and Lac has also been observed in a few cases.

Volume localized proton MRS has also been used to study the processes like glycolysis and lipid metabolism in muscle[125,126]. The spectra from muscle tissue exhibit two compartments of lipid signals with a difference of 0.2 ppm in their resonance frequencies[127]. These two compartments arise from intramyocellular (IMCL) and extramyocellular (EMCL) compartments of lipids. The useful-

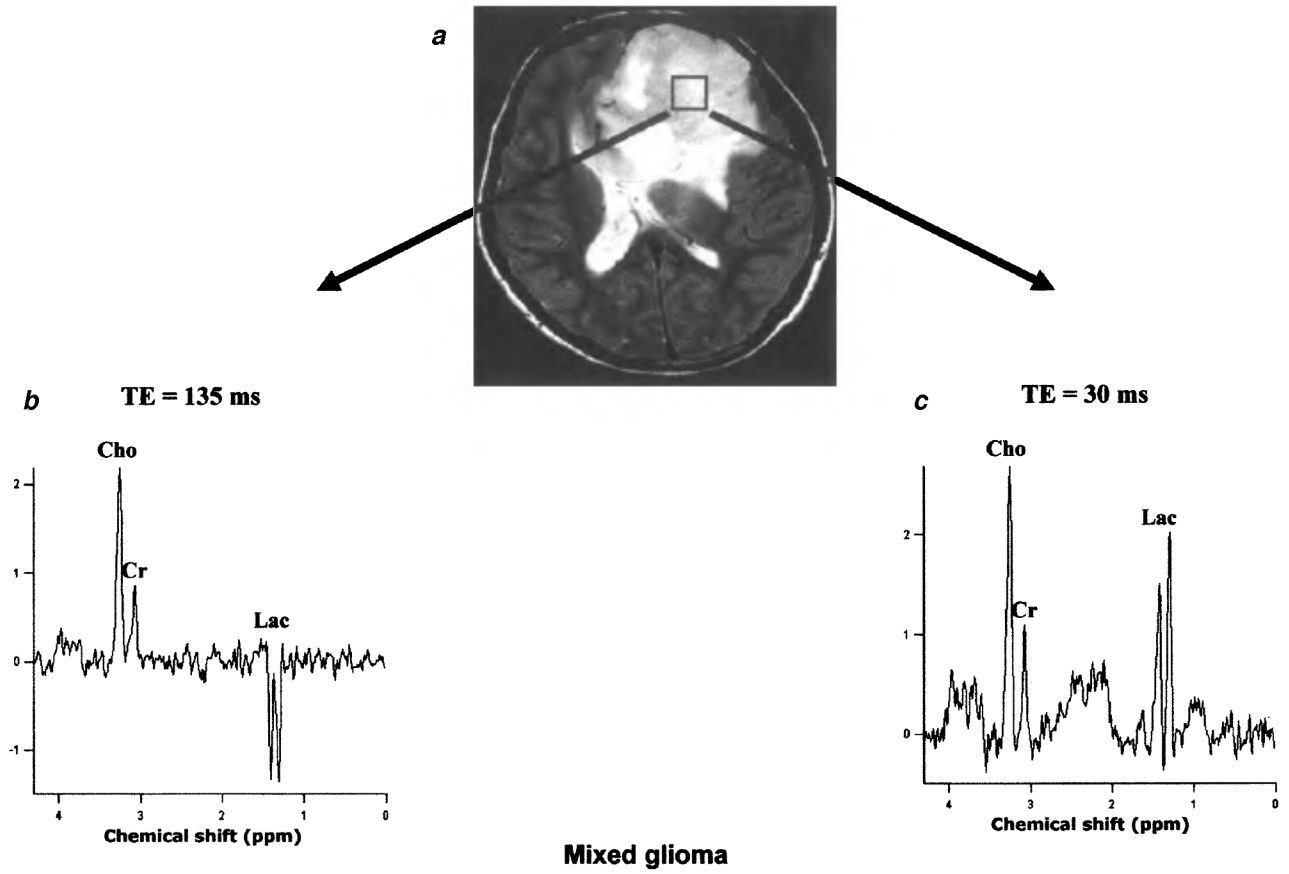

Figure 12. *a*, T2-weighted axial MR image (TR = 2500 ms; TE = 90 ms; slice thickness = 4 mm; FOV = 230 mm) of a patient suffering from brain mixed glioma. Proton spectrum from an 8 ml voxel positioned in the tumour region recorded at an echo time of TE = 135 ms (*b*) and TE = 30 ms (*c*).

ness of *in vivo* ^{1}H MRS in the study of polio patients has also been demonstrated[128]. It is reported that mildly paralysed patients are comparable with control subjects in relation to the presence of IMCL while moderate and severely paralysed patients were comparable in relation to the absence of IMCL. In addition, there is reduction or complete absence of creatine, carnitine and choline metabolites in severely paralysed patients[128].

In vivo proton MRS has been used for noninvasive detection of the biochemical differences between malignant and normal breast tissues in breast cancer patients that has been the recent interest in a few select laboratories. The spectrum from the tumour tissue is different from the normal and the unaffected breast tissues. In tumour, the water peak dominates with a much lower contribution from the protons of the fatty acid chains in comparison to the control and the unaffected breast. Comparison of water-to-fat (W/F) ratio among the above three groups showed that the tumours are characterized by high W/F values[129,130] which varied from 1 to 30, while in controls the value is 0.34 ± 0.25 and in the unaffected contralateral breast tissue of the breast cancer patients it is 0.35 ± 0.42. The W/F ratio can also be used to monitor the efficacy of the treatment procedures in breast cancer patients. A statistically significant reduction in the W/F ratio is noticed in patients who have undergone the full course of chemotherapy regimen (1.2 ± 1.5) compared to the pre-therapy value of 7.2 ± 7.4.

In the water suppressed proton spectra of breast cancer patients that in addition to the residual water and lipid, a peak due to choline containing compounds was observed. The intensity of the Cho peak was monitored prior to and one week after the completion of the 3rd and or 6th cycle of neoadjuvant chemotherapy for assessment of the effect of the therapy in many breast cancer patients[131]. Cho was found to be either reduced or absent in patients receiving full course of chemotherapy indicating response to chemotherapy[131]. The sensitivity of *in vivo* MRS in detecting Cho was 78% and the specificity was 86%.

Fluorine (^{19}F) MRS

Human body contains no fluorine and hence acts as a perfect tracer for MR studies. Moreover due to high signal strength (sensitivity, i.e. 83% of ^{1}H) and 100% natural abundance, this nucleus is appropriate for studying metabolism of fluorine containing drugs[132]. There are many drugs such as 5-fluorouracil (5-FU) and fluoropyrimidines, which are widely used in the treatment of human cancers, especially of gastrointestinal tract, breast and ovary. Metabolism of 5-FU in animal models[116,133] and humans has been studied[134,135]. Sequential ^{19}F NMR study[134] of breast cancer patients revealed that modulators like methotrexate and levamisole of 5-FU do not significantly increase the response rate of 5-FU. ^{19}F MRS has also been used to determine the concentration levels of antipsychotic drugs such as trifluoperazine and fluphenazine and antidepressant fluoroxetine[135,136].

Lithium (^{7}Li) MRS

^{7}Li has a spin 3/2 and a sensitivity of about 27% of ^{1}H and it typically gives a single narrow line in most biological systems arising from the Li cation present in both the intracellular and extracellular environments. Lithium salts are used with considerable success in alleviating or preventing both depressive and recurrences in manic depressive illness. By measuring the Li signal using *in vivo* MRS methods, pharmacokinetics and mechanism of action of Li containing drugs can be studied. The levels of Li in the muscle, serum and blood were monitored in patients suffering from manic-depressive illness with an episode of hypomania[137,138].

Conclusion

The progress in the application of various MR techniques in medicine has been unabated in the past two decades and has achieved an amazing level of success as an important tool through MRI and *in vivo* MRS to study the pathophysiology of several disease processes. This is due to its noninvasive nature, avoidance of ionizing radiation and its ability to generate high-resolution images. The development of various new imaging methodologies such as diffusion and perfusion imaging, real time functional MRI, contrast enhanced MRA, etc. has helped the physicians and the surgeons in diagnosis and management of various diseases, more objectively.

With rapid progress in the technology the goal of obtaining noninvasive biopsy information has pushed the development of interventional MRI and several optimized localized MRS procedures with water suppression and editing techniques. In fact, *in vivo* MRS is regularly used as a unique means to probe the biochemistry of living systems with diagnostic importance because of its ability to measure endogenous metabolites noninvasively and changes in tissue metabolism. Additional information about the biochemistry and physiology of living tissues, besides using ^{1}H and ^{31}P, can be obtained with many other nuclei like ^{19}F, ^{23}Na, ^{39}K and ^{13}C. The technique can also be used for measuring the distribution and pharmacokinetics of drugs *in vivo*. The sensitivity and specificity of *in vivo* MRS for several disease patterns particularly for small lesions need to be improved before MRS can be incorporated into clinical practice. The data from MRS is presently used as complementary information to that obtained from histology, mammogram and other accepted techniques. However, once MRS becomes established for clinical use unambiguously in one disease, it can be expected that the available technology will be more rapidly

be applied to other diseases. In fact, MRS has great clinical impact in localization of foci and brain damage in epilepsy and represents a valuable complement to conventional imaging techniques such as CT and MRI. The increased availability of 3 T and 4 T magnets would further enhance the spectral quality, particularly for proton MRS, fMRI and diffusion imaging studies. The ability to perform MRI and MRS noninvasively in the same setting with the same equipment without the injection of radioactive isotopes or blood sampling provides a considerable advantage in patient care as well as in improving our understanding of the pathophysiology of several diseases.

1. Damadian, R., Tumor detection by nuclear magnetic resonance. *Science*, 1971, **171**, 1151–1153.
2. Lauterbur, P. C., Image formation by induced local interaction: examples employing nuclear magnetic resonance. *Nature*, 1973, **242**, 190–191.
3. Mansfield, P. and Maudsley, A. A., Planar and line-scan spin imaging by NMR. Proc. XIXth Congress Ampere, Heidelberg, 1976, pp. 247–252.
4. Andrew, E. R., Bottomley, P. A., Hinshaw, W. S., Holland, G. N., Moore, W. S. and Simoraj, C., NMR images by the multiple sensitive point method: application to larger biological systems. *Phys. Med. Biol.*, 1977, **22**, 971–974.
5. Stark, D. D. and Bradley W. G., *Magnetic Resonance Imaging*, Mosby, New York, 1998.
6. Argov, Z., Lofberg, M. and Arnold, D. L., Insights into muscle diseases gained by phosphorus magnetic resonance spectroscopy. *Muscle Nerve*, 2000, **23**, 1316–1334.
7. Jagannathan, N. R., MR Imaging and Spectroscopy in Pharmaceutical and Clinical Research, Jaypee Brothers, New Delhi, 2001.
8. Gadian, D. G., *NMR and its Application to Living Systems*, Clarendon, Oxford, 1982.
9. Gunther, H., *NMR Spectroscopy, Basic Principles, Concepts and Applications in Chemistry* John Wiley, New York, 1982.
10. Mukherji, S. K., *Clinical Applications of Magnetic Resonance Spectroscopy*, John Wiley, New York, 1998.
11. Danielsen, E. R. and Ross, B. D., *Magnetic Resonance Spectroscopy Diagnosis of Neurological Diseases*, Marcel Dekker, New York, 1999.
12. Young, I. R. and Charles, H. C., *MR Spectroscopy Clinical Applications and Techniques*, Martin Dunitz, Cambridge, 1996.
13. Edelman, R. R., Hesselink, J. R. and Zlatkin, M. B., *Clinical Magnetic Resonance Imaging*, W B Saunders, Philadelphia, 1995, 2nd edn.
14. Arlert, I. P., Bougertz, G. N. and Manchal, G., *Magnetic Resonance Angiography*, Springer, Berlin, 1996.
15. Duerinckx, A. J., Coronary MR angiography. *Radiol. Clin. N. Am.*, 1996, **37**, 273–318.
16. Le Bihan, D., *Diffusion and Perfusion Magnetic Resonance Imaging,* Raven Press, New York, 1985.
17. Noris, D. G., Implications of bulk motion for diffusion-weighted imaging experiments: effects, mechanisms, and solutions. *J. Magn. Reson. Imaging*, 2001, **13**, 486–495.
18. Le Bihan, D., Mangin, J. F., Poupon, C., Clark, C. A., Pappata, S., Molko, N. and Chabriat, H., Diffusion tensor imaging: concepts and applications. *J. Magn. Reson. Imaging,* 2002, **13**, 534–546.
19. Ozscunar, Y. and Sorensen, A. G., Diffusion- and perfusion-weighted MRI in human acute ischaemic stroke: technical considerations. *Top. Magn. Reson. Imaging*, 2000, **11**, 259–272.
20. Molko, N. and Chabriat, H., Diffusion tensor imaging: concepts and applications. *J. Magn. Reson. Imaging,* 2001, **13**, 534–546.
21. Qui, H., M. S., Hedlund, L. W., Gewalt, S. L., Benveniste, H., Bare, T. M. and Johnson, G. A., Progression of a focal ischaemic lesion in rat brain during treatment with a novel glycine/NMDA antagonist: An *in vivo* 3D diffusion weighted MR microscopy study. *J. Magn. Reason. Imaging*, 1997, **7**, 739–744.
22. Sinha, K., Degaonkar, M. N., Jagannathan, N. R. and Gupta, Y. K., Effect of melatonin on ischaemic reperfusion injury induced by middle cerebral artery occlusion in rats. *Eur. J. Pharmacol.*, 2001, **428**, 185–192.
23. Gupta, Y. K., Singh, K., Choudhary, G. and Jagannathan, N. R., Protective effect of adenosine against neuronal injury induced by middle cerebral artery occlusion as evident by diffusion weighted imaging. *Pharm. Biochem. Behav.*, 2002, **72**, 569–572.
24. Degaonkar, M. N., Khubchandani, M., Dhawan, J. D., Jayasundar, R. and Jagannathan, N. R., Sequential proton MRS study of brain metabolite changes monitored during a complete pathological cycle of demyelination and remyelination in a lysophosphatidyl choline (LPC)-induced experimental demyelinating lesion model. *NMR Biomed.*, 2002, **15**, 293–300.
25. Barbier, E. L., Lamalle, L. and Decorps, M., Methodology of brain perfusion imaging. *J. Magn. Reson. Imaging,* 2001, **13**, 496–520.
26. Ogawa, S., Lee, T. M., Nayak, A. S. and Glynn, P., Oxygenation-sensitive contrast in magnetic resonance imaging of rodent brain at high fields. *Magn. Reson. Med.*, 1990, **4**, 68–78.
27. Ogawa, S., Lee, T. M., Kay, A. R. and Tank, D. W., Brain magnetic resonance imaging with contrast dependent on blood oxygenation. *Proc. Natl. Acad. Sci. USA*, 1990, **87**, 9868–9872.
28. Kim, S. G. and Ugurbil, K., Functional magnetic resonance imaging of the human brain. *J. Neurosci. Methods*, 1997, **74**, 229–243.
29. Kwong, K. K. *et al.*, Dynamic magnetic resonance imaging of human brain activity during primary sensory stimulation. *Proc. Natl. Acad. Sci. USA*, 1992, **89**, 5951–5955.
30. Detre, J. A. and Floyd, T. F., Functional MRI and its applications to the clinical neurosciences. *Neuroscientist*, 2001, **7**, 64–79.
31. Raichle, M. E., Functional brain imaging and human brain function. *J. Neurosci.*, 2003, **23**, 3959–3962.
32. Turner, R., Le Bihan, D., Moonen, C. T., Despres, D. and Frank, J., Echo planar time course MRI of cat brain oxygenation changes. *Magn. Reson. Med.*, 1991, **22**, 159–166.
33. Belliveau, J. W. *et al.*, Functional mapping of the human visual cortex by magnetic resonance imaging. *Science*, 1991, **254**, 716–719.
34. Kwong, K. K. *et al.*, Dynamic magnetic resonance imaging of human brain activity during primary sensory stimulation. *Proc. Natl. Acad. Sci. USA*, 1992, **89**, 5675–5679.
35. Bandettini, P. A., Wong, E. C., Hinks, R. S., Tikofsky, R. S. and Hyde, J. S., Time course EPI of human brain function during task activation. *Magn. Reson. Med.*, 1992, **25**, 390–397.
36. Ogawa, S. *et al.*, Intrinsic signal changes accompanying sensory stimulation: Functional brain mapping with magnetic resonance imaging. *Proc. Natl. Acad. Sci. USA*, 1992, **89**, 5951–5955.
37. Fox, P. T. and Raichle, M. E., Focal physiological uncoupling of cerebral blood flow and oxidative metabolism during somatosensory stimulation in human subjects. *Proc. Natl. Acad. Sci. USA*, 1986, **83**, 1140–1144.
38. Kim, S. G., Ashe, J., Hendrich, K., Ellermann, J. M., Merkle, H., Ugurbil, K. and Georgopoulos, A. P., Functional magnetic resonance imaging of motor cortex: hemispheric asymmetry and handedness. *Science*, 1993, **261**, 615–617.
39. Ruggieri, P. M. and Najm, I. M., MR imaging in epilepsy. *Neurol. Clin.*, 2001, **19**, 477– 489.
40. Mattay, V. S. and Weinberger, D. R., Organization of the human motor system as studied by functional magnetic resonance imaging. *Eur. J. Radiol.*, 1999, **30**, 105–114.
41. Hinke, R. M. *et al.*, Functional magnetic resonance imaging of Broca's area during internal speech. *Neuroreport,* 1993, **4**, 675–678.

42. Benson, R. R. *et al.*, Language dominance determined by whole brain functional MRI in patients with brain lesions. *Neurology*, 1999, **52**, 798–809.
43. Binder, J. R. *et al.*, Determination of language dominance using functional MRI: a comparison with the Wada test. *Neurology*, 1996, **46**, 978–984.
44. Small, S. L. and Burton, M. W., Functional magnetic resonance imaging studies of language. *Curr. Neurol. Neurosci. Rep.*, 2002, **2**, 1–16.
45. Halpern, D. F., *Sex Differences in Cognitive Abilities*, Erlbaum, Hillsdale, 1992, 2nd edn.
46. Shaywitz, B. A. *et al.*, Sex differences in the functional organization of the brain for language. *Nature*, 1995, **373**, 607–609.
47. Frahm, J., Bruhn, H., Merboldt, K. D. and Hanicke, W., Dynamic MR imaging of human brain oxygenation during rest and photic stimulation. *J. Magn. Reson. Imaging*, 1992, **2**, 501–505.
48. Tootell, R. B. H. *et al.*, Functional analysis of V3A and related areas in human visual cortex. *J. Neurosci.*, 1997, **17**, 7060–7078.
49. Le Bihan, D. (ed.), *Diffusion and Perfusion Magnetic Resonance Imaging: Applications to Functional MRI*. Raven, New York, 1995.
50. Beach, F. A. and Holz-Tucker, A. M., Effects of different concentrations of androgen upon sexual behaviour in castrated male rats. *J. Comp. Physiol.*, 1949, **42**, 433–453.
51. Tandon, S., An fMRI study to localize the brain areas involved in post-ejaculatory refractory period in human subjects. M.Sc. thesis, All India Institute of Medical Sciences, New Delhi, 2003.
52. Jackson, G. D., New techniques in magnetic resonance and epilepsy. *Epilepsia*, 1994, **35**, S2–S13.
53. Sheth, R. D., Epilepsy surgery: Presurgical evaluation. *Neurol. Clin.*, 2002, **20**, 1195–1215.
54. Detre, J. A., Sirven, J. I., Alsop, D. C., O'Connor, M. J. and French, J. A., Localization of sub-clinical activity by functional magnetic resonance imaging: correlation with invasive monitoring. *Ann. Neurol.*, 1995, **38**, 618–624.
55. Weiss, A. P. and Heckers, S., Neuroimaging of hallucinations: a review of the literature. *Psychiatry Res.*, 1999, **20**, 61–74.
56. Meisenzahl, E. M. and Schlosser, R., Functional magnetic resonance imaging research in psychiatry. *Neuroimaging Clin. N. Am.*, 2001, **11**, 365–374.
57. Callicott, J. H., An expanded role for functional neuroimaging in schizophrenia. *Curr. Opin. Neurobiol.*, 2003, **13**, 256–260.
58. Lin, S. P., Song, S. K., Miller, J. R., Ackermann, J, J. and Nei, J. J., Direct longitudinal comparison of ^{1}H and ^{23}Na MRI after transient focal cerebral ischaemia. *Stroke*, 2001, **32**, 925–932.
59. Sandstede, J. J. *et al.*, Assessment of myocardial infarction in humans with Na-23 MR imaging; comparison with cine MR imaging and delayed contrast enhancement. *Radiology*, 2001, **221**, 222–228.
60. Shapiro, E. M., Borthakur, A., Gougoutas, A. and Reddy, R., ^{23}Na MRI accurately measures fixed charge density in articular cartilage. *Magn. Reson. Med.*, 2002, **47**, 284–291.
61. McIntyre, D. J. O., Mccoy, C. L. and Griffiths, J. R., Tumor oxygenation measurements by ^{19}F magnetic resonance imaging of perfluorocarbons. *Curr. Sci.*, 1999, **76**, 753–762.
62. Albert, M. S., Cates, G. D., Drienhuys, B., Rapper, W., Saam, B., Springer, O. S. and Wishnia, A., Biological magnetic resonance imaging using laser polarized ^{129}Xe. *Nature*, 1994, **370**, 199–201.
63. Ebert, N. *et al.*, Nuclear magnetic resonance image with hyper polarized helium. *Lancet*, 1996, **147**, 1297–1299.
64. Albert, M., Cates, G. D., Driehys, B., Happer, W, Saan, B., Springer, C. S. Jr. and Wizhaia, A., Biological magnetic resonance imaging using laser-polarized ^{129}Xe. *Nature*, **370**, 199–201.
65. Kauczor, H. U., Surkau, R. and Roberts, T., MRI using hyperpolarized noble gases. *Eur. J. Radiol.*, 1998, **8**, 820–827.
66. McAdams, H. P., Hatabu, H., Donnelly, L. F., Chen O Tadamura, E. and MacFall, J. R., Novel techniques for MR imaging of pulmonary air spaces. *Magn. Reson. Imaging Clin. N. Am.*, 2000, **8**, 205–219.
67. Salerno, M., Altes, T. A., Mugler, J. P., Nakatsu, M., Hatubu, H. and De Lange, E. E., Hyperpolarized noble gas MR imaging of the lung: potential clinical applications. *Eur. J. Radiol.*, 2001, **40**, 33–44.
68. Buonano, F. S. *et al.*, Proton NMR imaging in experimental ischaemic infarction. *Stroke*, 1983, **14**, 173–177.
69. Sauter, P., Rudin, M. and Wiederhold, K. H., Reduction of neural damage in irreversible cerebral ischaemia by calcium antagonists. *Neurochem. Pathol.*, 1988, **9**, 211–236.
70. Sauer, D., Allegrini, P. R. and Fagg. G. E., The competitive NMDA antagonist CGP 40116 is a potent neuroprotectant in a rat model of focal cerebral ischaemia. *J. Neural. Trans. Suppl.*, 1994, **43**, 81–89.
71. Sauter, A. and Rudin, M., Calcium antagonists for reduction of brain damage in stroke. *J. Cardiovasc. Pharmac.* (*Suppl. 1*), 1990, **15**, 543–547.
72. Muruganandham, M., Kasiviswanathan, A., Jagannathan, N. R., Raghunathan, P., Jain, P. C. and Jain, V., Diltiazem enhances tumour blood flow: MRI study in a murine tumour. *Int. J. Radiat. Oncol. Biol. Phys.*, 1999, **43**, 413–421.
73. Koretsky, A. P., Brosnan, M. J., Chen, L, Chen, J. and Van Dyke, T., NMR determination of creatine kinase expressed in liver of transgenic mice: Determination of free ADP levels. *Proc. Natl. Acad. Sci. USA*, 1990, **87**, 3112–3116.
74. Roman, B. B., Foley, J. M., Meyer, R. A. and Koretsky, A. P., Contractile and metabolic effects of increased creatine kinase activity in mouse skeletal muscle. *Am. J. Pathol.*, 1996, **270**, C1236–1245.
75. Jolesz, F. A. and Young, I. R. (eds), *Interventional MR: Techniques and Clinical Experience*, London, Martin Dunitz, 1998.
76. Hore, P. J., Solvent suppression in Fourier transform nuclear magnetic resonance. *J. Magn. Reson.*, 1983, **55**, 283–300.
77. Dumoulin, C. L., A method of chemical-shift selective imaging. *Magn. Reson. Med.*, 1985, **2**, 583–585.
78. Haase, A., Frahm, J., Hanicke, W. and Matthei, D., ^{1}H NMR chemical shift selective (CHESS) imaging. *Phys. Med. Biol.*, 1985, **30**, 341–344.
79. Frahm, J., Merboldt, K. D. and Hanicke, W., Localized proton spectroscopy using stimulated echoes. *J. Magn. Reson.*, 1987, **72**, 502–508.
80. Frahm, J., Bruhn, H., Gyngell, M. L., Merboldt, K. D., Hanicke, W. and Sauter, R., Localized high-resolution proton NMR spectroscopy using stimulated echoes: initial application to human brain *in vivo*. *Magn. Reson. Med.*, 1989, **9**, 79–93.
81. Bottomley, P. A., Selective volume method for performing localized NMR spectroscopy. *U S Patent*, 1984, 4, **480**, 228.
82. Ordidge, R. J., Bendall, M. R., Gordon, R. E. and Connelly, A., Volume selection for *in vivo* biological spectroscopy. In *Magnetic Resonance in Biology and Medicine* (eds Govil, G., Khetrapal, C. L. and Saran, A., Tata McGraw Hill, New Delhi, 1985, pp. 387– 397.
83. Brown, T. R., Kincaid, B. M. and Ugurbil, K., NMR chemical shift imaging in three dimensions. *Proc. Natl. Acad. Sci. USA*, 1982, **79**, 3523–3526.
84. Maudsley, A. A., Hilal, S. K., Perman, W. H. and Simon, H. E., Spatially resolved high resolution spectroscopy by 'four dimensional' NMR. *J. Magn. Reson.*, 1983, **51**, 147–152.
85. Bottomley, P. A., Charles, H. C., Roemer, P. B., Falmig, D., Engeseth, H., Edelstein, W. A. and Mueller, O. M., Human *in vivo* phosphate metabolite imaging with ^{31}P NMR. *Magn. Reson. Med.*, 1988, **7**, 319–336.
86. Twieg, D. B. *et al.*, Localized ^{31}P MRS in humans by spectroscopic imaging. *Magn. Reson. Med.*, 1989, **12**, 291–305.
87. Segebarth, C. M., Baleriaux, D. F., Luyten, P. R. and Hollander, J. A., den., Detection of metabolic heterogeneity of human intracranial tumours *in vivo* by ^{1}H NMR spectroscopic imaging. *Magn. Reson. Med.*, 1990, **13**, 62–76.

88. Luyten, P. R. *et al.*, Metabolic imaging of patients with intracranial tumours ^{1}H MR spectroscopic imaging and PET. *Radiology*, 1990, **176**, 791–799.
89. Segebarth, C. M., Baleriaux, D., Arnold, D. A., Luyten, P. R. and Hollander, J. A. den., MR image-guided ^{31}P MR spectroscopy in the evaluation of brain tumour treatment. *Radiology*, 1987, **165**, 215–219.
90. Maris, J., Evans, A., Mclaughlin, A., Angio, G. J. D., Bolinger, L., Manos, H. and Chance, B., ^{31}P NMR spectroscopic investigation of human neuroblastoma *in situ*. *N. Engl. J. Med.*, 1985, **312**, 1500–1505.
91. Hope, P. L. *et al.*, Cerebral energy metabolism studied with phosphorus NMR spectroscopy in normal and birth-asphyxiated infants. *Lancet*, 1984, **2**, 366–370.
92. Younkin, D. P., Delivoria-Papadopoulos, M., Leonard, J. C., Subramanian, V. H., Eleff, S., Leigh, Jr. J. S. and Chance, B., Unique aspects of human newborn cerebral metabolism evaluated with phosphorus nuclear magnetic resonance spectroscopy. *Ann. Neurol.*, 1984, **16**, 581–586.
93. Boesch, D., Gruetter, R., Martin, E., Duc, G. and Wuthrich, K., Variations in the *in vivo* ^{31}P MR spectra of the developing human brain during postnatal life. Work in progress. *Radiology*, 1989, **172**, 197–199.
94. Podo, F., Tumor phospholipid metabolism. *NMR Biomed.*, 1999, **12**, 413–439.
95. Argov, Z., Lofberg, M. and Arnold, D. L., Insights into muscle diseases gained by phosphorus magnetic resonance spectroscopy. *Muscle Nerve*, 2000, **23**, 1316–1334.
96. Kutsuzawa, T., Shioya, S., Kurita, D., Haida, M. and Yamabayashi, H., Effects of age on muscle energy metabolism and oxygenation in the forearm muscle. *Med. Sci. Sports Exer.*, 2001, **33**, 901–906.
97. Gupta, R. K., Mittal, R. D., Aggarwal, K. N. and Agarawal, D. K., Muscular sufficiency, serum protein, enzymes and bioenergetic studies (^{31}P magnetic resonance spectroscopy) in chronic malnutrition. *Acta. Pediaet.*, 1994, **83**, 327–331.
98. Thompson, A., Damyanovich, A., Madapallimattam, A., Mikalus, D., Allord, J. and Jeejeebhoy, K. N., ^{31}P-nuclear magnetic studies of bioenergetic changes in skeletal muscle in malnourished human adults. *Am. J. Clin. Nutr.*, 1998, **67**, 39–43.
99. Taylor, D. J., Clinical utility of muscle MR spectroscopy. *Semin. Musculoskel. Radiol.*, 2000, **4**, 481–502.
100. Heerschap, A., Houtman, C., Zandt in't H. J., Bergh van den, A. J. and Wieringa, B., Introduction to *in vivo* ^{31}P magnetic resonance spectroscopy of (human) skeletal muscle. *Proc. Nutr. Soc.*, 1999, **58**, 861–870.
101. Barbiroli, B., Funicello, R., Iotti, S., Montagna, P., Ferlini, A. and Zaniol, P., ^{31}P NMR spectroscopy of skeletal muscle in Becker dystrophy and DMD/BMD carriers. Altered rate of phosphate transport. *J. Neurol. Sci.*, 1992, **109**, 188–195.
102. Barbiroli, B., Funicello, R., Ferlini, A., Montagna, P. and Zaniol, P., Muscle energy metabolism in female DMD/BMD carriers: a ^{31}P-MR spectroscopy study. *Muscle Nerve*, 1992, **15**, 344–348.
103. Kemp, G. J., Taylor, D. J., Dunn, J. F., Frostick, S. P. and Radda, G. K., Cellular energetics of dystrophic muscle. *J. Neurol. Sci.*, 1993, **116**, 201–206.
104. Ronen, S. M. and Leach, M. O., Imaging biochemistry: applications to breast cancer. *Breast Cancer Res.*, 2001, **3**, 36–40.
105. Leach, M. O. *et al.*, Measurements of human breast cancer using magnetic resonance spectroscopy: a review of clinical measurements and a report of localized ^{31}P measurements of response to treatment. *NMR Biomed.*, 1998, **11**, 314–340.
106. Miller, B. L., A review of chemical issues in 1H NMR spectroscopy: N-acetyl-aspartate, creatine and choline. *NMR Biomed.*, 1991, **4**, 47–52.
107. Fleming, M. C. and Lowry, O. H., The measurement of free and N-acetylated aspartic acid in the nervous system. *J. Neurochem.*, 1996, **13**, 779–783.
108. Ross, B. D. and Michaelis, T., Clinical applications of magnetic resonance spectroscopy. *Mag. Res. Q.*, 1994, **10**, 191–247.
109. Ross, B. D., Biochemical considerations in ^{1}H spectroscopy. Glutamate, glutamine, myo-inositol and related metabolites. *NMR Biomed.*, 1991, **4**, 59–63.
110. Miller, B. L., Moats, R. A., Shonk, T., Ernst, T., Wolley, S. and Ross, B. D. Alzheimer diseases: Depiction of increased cerebral myo-inositol with proton MR spectroscopy. *Radiology*, 1993, **187**, 433–437.
111. Castillo, M., Kwock, L. and Mukherji, S. K., Clinical applications of proton MR spectroscopy. *AJNR Am. J. Neuroradiol.*, 1996, **17**, 1–15.
112. Burtscher, I. M. and Holtas, S., Proton magnetic resonance spectroscopy in brain tumours: clinical applications. *Neuroradiology*, 2001, **43**, 345–352.
113. Leclerc, X. Huisman and Sorensen, A. G., The potential of proton magnetic resonance spectroscopy (^{1}H-MRS) in the diagnosis and management of patients with brain tumours. *Curr. Opin. Oncol.*, 2002, **14**, 292–298.
114. Ishimaru, H., Morikawa, M., Iwanaga, S., Kaminogo, M., Ochi, M. and Hayashi, K., Differentiation between high-grade glioma and metastatic brain tumour using single voxel proton MR spectroscopy. *Eur. J. Radiol.*, 2001, **11**, 1784–1791.
115. Herminghaus, S., Pilatus, U., Moller-Hartmann, W., Raab, P., Lanfermann, H., Scholte, W. and Zanella, F. E., Increased choline levels coincide with enhanced proliferative activity of neuroepithelial brain tumours. *NMR Biomed.*, 2002, **15**, 385–392.
116. Sijens, P. E. *et al.*, ^{1}H MR spectroscopy in patients with metastatic brain tumours: a multicenter study. *Magn. Reson. Med.*, 1995, **33**, 818–826.
117. Tarnaswki, R., Sokol, M., Pieniazek, P., Maciejewski, B., Walecki, J., Miszczyk, L. and Krupska, T., ^{1}H-MRS *in vivo* predicts the early treatment outcome of postoperative radiotherapy for malignant gliomas. *Int. J. Radiat. Oncol. Biol. Phys.*, 2002, **52**, 1271–1276.
118. Graham, G. D., Hwang, J. H., Rothman, D. L. and Prichard, J. W., Spectroscopic assessment of alterations in macromolecule and small molecule metabolite in human brain after stroke. *Stroke*, 2001, **32**, 2797–2802.
119. Gupta, R. K. *et al.*, Relationships between choline magnetic resonance spectroscopy, apparent diffusion coefficient and quantitative histopathology in human glioma. *J. Neurooncol.*, 2000, **50**, 215–226.
120. Jayasundar, R., Singh, V. P., Jain, V., Raghunathan, P. and Banerji, A. K., Inflammatory granulomas: evaluation with proton MRS. *NMR Biomed.*, 1999, **12**, 139–144.
121. Jagannathan, N. R., Desai, N. G. and Raghunathan, P., Brain metabolite changes in alcoholism: an *in vivo* proton magnetic resonance spectroscopy (MRS) study. *Magn. Reson. Imaging*, 1996, **14**, 553–557.
122. Jagannathan, N. R., Tandon, N., Raghunathan, P. and Kochupillai, N., Reversal of abnormalities of myelination by thyroxin therapy in congenital hypothyroidism: localized *in vivo* proton magnetic resonance spectroscopy (MRS) study. *Dev. Brain Res.*, 1998, **109**, 179–186.
123. Stanley, J. A., *In vivo* magnetic resonance spectroscopy and its application to neuropsychiatric disorders. *Can. J. Psychiatry*, 2002, **47**, 315–326.
124. Kasai, K., Iwanami, A., Yamasue, H., Kuroki, N., Nakagome, K. and Fukuda, M., Neuroanatomy and neurophysiology in schizophrenia. *Neurosci. Res.*, 2002, **43**, 93–110.
125. Auer, D. P., Wilke, M., Grabner, A., Heidenreich, J. O., Bronisch, T. and Wetter, T. C., Reduced NAA in the thalamus and altered membrane and glial metabolism in schizophrenic patients

detected by ^{1}H-MRS and tissue segmentation. *Schizophr. Res.*, 2001, **52**, 87–99.

126. Boesch, C. and Kreis, R., Observation of intracellular lipids by ^{1}H-magnetic resonance spectroscopy. *Ann. N. Y. Acad. Sci.*, 2000, **904**, 25–31.
127. Schick, F., Eismann, B., Jung, W. I., Bungers, H., Bunse, M. and Lutz, O., Comparison of localized proton NMR signals of skeletal muscle and fat tissue *in vivo*: two lipid compartments in muscle tissue. *Magn. Reson. Med.*, 1993, **29**, 158–167.
128. Jagannathan, N. R. and Wadhwa, S., *In vivo* proton magnetic resonance spectroscopy (MRS) study of post polio residual paralysis (PPRP) patients. *Magn. Reson. Imaging*, 2002, **20**, 113–117.
129. Jagannathan, N. R., Singh, M., Govindaraju, V., Raghunathan, P., Coshic, O., Julka, P. K. and Rath, G. K., Volume localized *in vivo* proton MR spectroscopy of breast carcinoma: variation of water-fat ratio in patients receiving chemotherapy. *NMR Biomed.*, 1998, **11**, 414–422.
130. Jagannathan, N. R., Kumar, M., Raghunathan, P., Coshic, O., Julka, P. K. and Rath, G. K., Assessment of the therapeutic response of human breast carcinoma using *in vivo* volume localized proton magnetic resonance spectroscopy. *Curr. Sci.*, 1999, **76**, 777–782.
131. Jagannathan, N. R., Seenu, V., Coshic, O., Dwivedi, S. N., Julka, P. K., Srivastava, A. and Rath, G. K., Evaluation of total choline from *in vivo* volume localized proton MR spectroscopy and its response to neoadjuvant chemotherapy in locally advanced breast cancer. *Br. J. Cancer*, 2001, **84**, 1016–1022.
132. Komoroski, R. A., Newton, J. E. O., Cardwell, D., Sprigg, J., Pearce, J. and Karson, C. N., *In vivo* ^{19}F spin relaxation and localized spectroscopy of fluoxetine in human brain. *Magn. Reson. Med.*, 1994, **31**, 204–211.
133. Stevens, A. N., Morris, P. G., Iies, R. A., Sheldon, P. W. and Griffiths, J. R., 5-Fluorouracil metabolism monitored by in-vivo ^{19}F NMR. *Br. J. Cancer*, 1985, **50**, 113–117.
134. Mohanakrishnan, P. *et al.*, Metabolism of 5-fluorouracil in human liver. An *in vivo* ^{19}F NMR study. *Curr. Sci.*, 1999, **76**, 677–680.
135. Wolf, W., Albright, M. J., Silver M. S., Weber, H., Reichardt, V. and Sauer, R., Fluorine-19 NMR spectroscopic studies of the metabolism of 5-flurouracil in the liver of patients undergoing chemotherapy. *Magn. Reson. Imaging*, 1987, **5**, 165–169.
136. Renshaw, P. F. *et al.*, Accumulation of fluoxetine and norfluoxetine in human brain during therapeutic administration. *Am. J. Psychiatry*, 1992, **149**, 1592–1594.
137. Gonzalez, R. G., Guimaraes, A. R., Sachs, G. S., Rosenbaum, J. F., Garwood, M. and Renshaw, P. F., Measurement of human brain lithium *in vivo* by MR spectroscopy. *Am. J. Neuroradiol.*, 1993, **14**, 1027–1037.
138. Komoroski, R. A., Newton, J. E. O., Walker, E., Cardwell, D., Jagannathan, N. R., Ramaprasad, S. and Sprigg, J., *In vivo* NMR spectroscopy of lithium-7 in humans. *Magn. Reson. Med.*, 1990, **15**, 347–356.

ACKNOWLEDGEMENTS. I thank the Department of Science and Technology, New Delhi for financial assistance for carrying out some of the work presented here. I also thank my students and other collaborators for their cooperation, help and many fruitful discussions.

Received and accepted 11 November 2003

Physiological functions of multidrug transporters in yeast

Rajendra Prasad† and Snehlata Panwar*

Membrane Biology Laboratory, School of Life Sciences, Jawaharlal Nehru University, New Delhi 110 067, India
*Present address: Department of Genetics, Cell Biology and Development, University of Minnesota, 6-160 Jackson Hall, 321 Church Street, Minneapolis, MN 55455, USA

Overexpression of drug extrusion pumps belonging to the ABC (ATP-binding cassette) super family of proteins is one of the most common mechanisms of multidrug resistance in various organisms. Both pathogenic and non-pathogenic yeast cells also become resistant to a variety of drugs by overexpressing genes encoding ABC drug efflux pumps. Recent evidences reveal that not only the well-characterized human drug extrusion pump (MDR1/P-gp), but its close homologues in yeast also mediate several cellular functions. Keeping in view the importance of ABC drug transporters in yeasts, this review particularly focuses on their physiological roles.

THE rapidly growing ATP-Binding Cassette (ABC) superfamily, also known as 'traffic ATPases', comprises an extremely diverse class of membrane-transport proteins[1–5]. These proteins, which were discovered almost two decades ago in bacteria as high-affinity nutrient transporters, shot to prominence when their ability to confer multidrug resistance (MDR) in cancer cells was realized[6]. Among several mechanisms that seem to contribute to the MDR phenomenon, overexpression of drug extrusion pumps belonging to the ABC superfamily is the most frequent cause of resistance to antifungals, herbicides, anticancer and cytotoxic drugs. To date, the most documented and well-characterized ABC drug extrusion pump has been the P-glycoprotein (human MDR1/P-gp) of tumour cells[6]. The presence of proteins homologous to human MDR1/P-gp in all organisms, ranging from the prokaryotes to eukaryotes, including yeasts and plants, portrays drug extrusion as a general mechanism of MDR.

ABC proteins can transport a variety of structurally diverse hydrophobic substrates[2]. The functional diversity of the ABC proteins is also reflected in their ever-emerging physiological roles in nutrient, peptide, lipid and cholesterol transport, the biosynthesis of molecules like heme, cell development in plants, apoptosis, and translational regulation[7–13]. Interestingly, human diseases such as cystic fibrosis, adrenoleukodystrophy, Dubin–Johnson syndrome, Tangier disease are associated with mutations in human genes encoding ABC transporters, which again reflects their relevance in cellular physiology[14,15]. In view of the above, a general question pertaining to the physiological importance of ABC drug-transporter proteins always comes up. It is expected that such a large family of transporters cannot be dedicated merely to drug efflux. This view is supported by the fact that very close homologues of the ABC proteins are not drug extrusion pumps, and mediate dedicated physiological functions. Studies dealing with physiological signals that control the expression of the drug extrusion pumps have also provided new insights not only into the complexities of regulatory circuits but also into the requirement of these pumps in normal cell functioning[16].

When challenged with antifungals and other drugs, both pathogenic and non-pathogenic yeasts have the capacity to overcome their inhibitory action through specific resistance mechanisms[17–23]. One of the most prominent resistance mechanisms includes overexpression of genes encoding drug extrusion pumps belonging to the ABC superfamily. In view of the limited scope of the article, we have not attempted to discuss the physiological functions mediated by all the ABC proteins of yeasts; rather we have focused on the cellular functions of only the drug extrusion pumps of this superfamily. How these pumps are involved in conferring multidrug resistance in yeasts is a widely reviewed subject and hence this aspect has not been discussed in this article[18–23].

Drug transporters of the ABC superfamily of yeasts

Yeast ABC transporters, like their mammalian homologues, possess specific domains for membrane association and ATP-binding and hydrolysis. A typical yeast ABC protein comprises of two homologous halves, each made up of a hydrophilic, cytoplasmic, nucleotide-binding domain (NBD) and a hydrophobic domain represented by six transmembrane stretches (TMS). In addition, the NBD consists of one Walker A, Walker B and a signature or C-motif. The completion of the *Saccharomyces cerevisiae* genome-sequence project led to the identification of 30 putative ABC proteins which are divided into six clusters, viz. the PDR, MDR, MRP/CFTR, RL1, YEF3 and ALDP subfamilies[14,24,25]. The PDR subfamily is the largest among these clusters and most of the drug transporters of *S. cerevisiae* belong to this subfamily of ABC proteins (discussed below). Table 1 lists only those ABC

*For correspondence. (e-mail: rp47@hotmail.com)